JAERI-M
86-172

DATA SET FOR BENCHMARK CALCULATION ON IDEAL MHD BETA LIMIT OF INTOR PLASMA

November 1986

Toshihide TSUNEMATSU, Shinji TOKUDA, Toshiyuki NEMOTO*
Masafumi AZUMI and Tatsuoki TAKEDA

日 本 原 子 力 研 究 所
Japan Atomic Energy Research Institute

JAERI-Mレポートは，日本原子力研究所が不定期に公刊している研究報告書です。
入手の問合わせは，日本原子力研究所技術情報部情報資料課（〒319-11 茨城県那珂郡東海村）あて，お申しこしください。なお，このほかに財団法人原子力弘済会資料センター（〒319-11 茨城県那珂郡東海村日本原子力研究所内）で複写による実費領布をおこなっております。

JAERI-M reports are issued irregularly.
Inquiries about availability of the reports should be addressed to Information Division Department of Technical Information, Japan Atomic Energy Research Institute, Tokaimura, Naka-gun, Ibaraki-ken 319-11, Japan.

編集兼発行　日本原子力研究所
印　　刷　日青工業株式会社

JAERI-M 86-172

Data Set for Benchmark Calculation on Ideal MHD Beta Limit of INTOR Plasma

Toshihide TSUNEMATSU, Shinji TOKUDA, Toshiyuki NEMOTO*

Masafumi AZUMI+ and Tatsuoki TAKEDA

Department of Thermonuclear Fusion Research

Naka Fusion Research Establishment

Japan Atomic Energy Research Institute

Naka-machi, Naka-gun, Ibaraki-ken

(Received October 17, 1986)

Data sets for the benchmark calculations of the ideal MHD beta limit are presented. These data sets are useful for the international collaborations such as INTOR workshop. For the detailed comparison of the results, the documentations of the basic equations and numerical methods are also described.

Keywords : Beta Limit, Benchmark Calculation, INTOR, MHD Equilibrium, Stability Analysis

+ Department of Large Tokamak Research

* on leave from Fujitsu Ltd.

JAERI－M　86－172

INTORプラズマのベータ値限界に関する ベンチマーク計算用データセット

日本原子力研究所那珂研究所核融合研究部
常松　俊秀・徳田　伸二・根本　俊行*・安積　正史+
竹田　辰興

（1986年10月17日受理）

本報告書は理想ＭＨＤ安定性から決まるトカマク・プラズマのベータ値限界計算のためのベンチマーク・データセットをまとめたものである。このデータセットはINTOR等国際核融合研究協力に於て有効に利用されている。各国提示結果の詳細な比較のために，計算の基礎方程式と数値計算法も併せて述べる。

那珂研究所：〒311-02　茨城県那珂郡那珂町大字向山801－1
+　臨界プラズマ研究部
*　外来研究員（富士通㈱）

CONTENTS

目　　次

1. Introduction

The ideal MHD beta limit is used to determine the beta limit of a reactor plasma. A lot of calculations have been carried out to assess the beta limit [1]. The results are approximately described as a simple scaling law [2] i.e, $\beta(\%)=gI_p(MA)/a(m)B_t(T)$, where I_p, a and B_t are the total plasma current, the horizontal minor radius and the toroidal magnetic field strength at the center of the plasma, and g is a constant of 3-4. The difference in g is considered to be due to the difference in the parameters in the calculations, e.g. the modes, profiles and plasma shapes. In the international collaboration for the design of a specific fusion reactor, such as INTOR workshops, it is necessary to clarify the cause of the differences for the assessment of the data base. If the difference comes from that in the definition of physical parameters or the numerical accuracy, the data base makes us confused. Benchmark calculations and the documentation of numerical codes are the first step to assess the data base which are presented by each delegation. In this report, we present the description of the equilibrium (SELENE40) and stability (ERATO-J) codes in JAERI and propose the data sets for the benchmark calculation on the ideal MHD beta limit.

2. Equilibrium calculation

2.1 Basic equations

In the axisymmetric toroidal system, the equilibrium magnetic field B and current J are written by the poloidal flux function $\psi(R,Z)$ in the cylindrical coordinates (R,Z,φ):

$$B = \nabla\varphi \times \nabla\psi + F\nabla\varphi \tag{1}$$

and

$$\mu_0 J = \Delta^*\psi\nabla\varphi + \nabla F\times\nabla\varphi \ , \tag{2}$$

1. Introduction

The ideal MHD beta limit is used to determine the beta limit of a reactor plasma. A lot of calculations have been carried out to assess the beta limit [1]. The results are approximately described as a simple scaling law [2] i.e, $\beta(\%)=gI_p(MA)/a(m)B_t(T)$, where I_p, a and B_t are the total plasma current, the horizontal minor radius and the toroidal magnetic field strength at the center of the plasma, and g is a constant of 3-4. The difference in g is considered to be due to the difference in the parameters in the calculations, e.g. the modes, profiles and plasma shapes. In the international collaboration for the design of a specific fusion reactor, such as INTOR workshops, it is necessary to clarify the cause of the differences for the assessment of the data base. If the difference comes from that in the definition of physical parameters or the numerical accuracy, the data base makes us confused. Benchmark calculations and the documentation of numerical codes are the first step to assess the data base which are presented by each delegation. In this report, we present the description of the equilibrium (SELENE40) and stability (ERATO-J) codes in JAERI and propose the data sets for the benchmark calculation on the ideal MHD beta limit.

2. Equilibrium calculation

2.1 Basic equations

In the axisymmetric toroidal system, the equilibrium magnetic field B and current J are written by the poloidal flux function $\psi(R,Z)$ in the cylindrical coordinates (R,Z,φ):

$$B = \nabla\varphi \times \nabla\psi + F\nabla\varphi \tag{1}$$

and

$$\mu_0 J = \Delta^*\psi\nabla\varphi + \nabla F\times\nabla\varphi \ , \tag{2}$$

where

$$\triangle^*\psi = R^2\nabla\cdot(\nabla\psi/R^2) = R\frac{\partial}{\partial R}\left(\frac{1}{R}\frac{\partial\psi}{\partial R}\right) + \frac{\partial^2\psi}{\partial Z^2} \quad . \tag{3}$$

The equation for MHD equilibria, $\nabla P=J\times B$, can be reduced to the Grad-Shafranov equation,

$$\triangle^*\psi = -R^2\mu_0\frac{dP}{d\psi} - \frac{1}{2}\frac{dF^2}{d\psi} = g(R,\psi) \quad \text{(in a plasma)} \tag{4a}$$

and

$$\triangle^*\psi = 0 \qquad \text{(in a vacuum)} \quad , \tag{4b}$$

when the plasma pressure is isotropic and the function of ψ. The poloidal current function , F ($F=RB_t$, B_t :toroidal magnetic field) is also the function of ψ. The functions P and F are arbitrary in eq.(4). The time-evolution of these functions are determined by a transport process. For the MHD stability analysis, P and F are given by using a simple model which is shown in §2.3 .

2.2 Plasma shape and boundary condition

The shape of a plasma surface is specified by the functions,

$$R = R_0 + a\cos(\theta+\delta^*\sin\theta) \quad , \tag{5a}$$

and

$$Z = \kappa a\sin\theta \quad , \tag{5b}$$

where R_0, κ and a are the major radius of the plasma center, the ellipticity and the minor radius, respectively. The parameter, δ^*, specifies the triangularity. The solution of the equation , $\triangle^*\psi_v=0$, gives the poloidal magnetic flux supplied by external coils (vacuum field solution). The general solutions, $\{\psi_{vi}\}$, are used to control a plasma shape. The vacuum flux is expressed by a linear combination of

the general solutions:

$$\psi_v = \sum_{i=1}^{M} C_i \psi_{vi} \quad . \tag{6}$$

The coefficients, $\{C_i\}$, are determined so that the flux contour with $\psi+\psi_v=\psi_s$ may pass the specified points on the plasma surface given by eq.(5), (ψ:the solution of the Grad-Shafranov equation, ψ_s: flux at the plasma surface). The condition that the contour with $\psi+\psi_v=\psi_s$ passes the specified points is too stringent for the coil systems in the design of experimental devices. For this purpose, a least square error can be minimized :

$$E = \sum_i a_i \mid (\psi+\psi_v)_i - \psi_{si} \mid^2 + \sum_i b_i I_i^2 = \min \ : \ , \tag{7}$$

where $\{a_i\}$, $\{b_i\}$ and I_i are the weights and the currents in the external coils. The Grad-Shafranov equation (eq.(4)) is solved in the rectangular domain , R^*, in the (R,Z) space (Fig.1). The poloidal flux function, ψ, is arbitrary by a constant which is chosen as $\psi_s=0$ at the plasma surface. By using this condition and the Green's theorem, the poloidal flux produced by a plasma current in a vacuum region is given by

$$\psi_p(r) = \oint_{\psi=0} G(r,r') \, B_p(R',Z') dl' \tag{8}$$

where

$$B_p = \mid \nabla\psi \mid \ / \ R \quad , \tag{9}$$

$$G(r,r') = -\frac{1}{2\pi} \sqrt{RR'} \ / \ k \cdot \{(2-k^2)K(k) - E(k)\}, \tag{10a}$$

and

$$k = \frac{4RR'}{(R+R')^2 + (Z-Z')^2}. \tag{10b}$$

The functions K(k) and E(k) are the first and second complete elliptic integral, respectively. The Grad-Shafranov equation is numerically

solved by using iterative method. The methods are described in §2.3. The boundary condition for the n-th iteration is given on the rectangular boundary, ∂R^*, by using the solution at the (n-1)th step;

$$\psi^n(\partial R^*) = \psi_p{}^{n-1}(\partial R^*) + \psi_v{}^n(\partial R^*) , \tag{11}$$

where $\psi_v{}^n$ is calculated by using the condition $\psi^{n-1}+\sum C_i\psi_{vi}=0$ at the specified points of the plasma surface. When the iteration converges, the solution in an unbounded domain is obtained.

2.3 Numerical Methods

2.3.1 Nonlinear Eigenvalue Problem

When the inhomogeneous term in eq.(4), $g(R,\psi)$, is given as the function of a normalized flux, $\bar{\psi}=1-\psi/\psi_0$ ($\psi_s=0$ and ψ_0 : poloidal magnetic flux at the axis), the semi-linear equation can be solved by using the algorithm of the nonlinear eigenvalue problem :

$$\Delta^*\psi^n = \lambda^n f(R,\bar{\psi}^{n-1}) \quad \text{(in a plasma)} \tag{12a}$$

$$\Delta^*\psi^n = 0 \quad \text{(in vacuum)} \tag{12b}$$

with the boundary condition described in §2.2 . Equation (12) can be solved numerically in a rectangular domain by using the double-cyclic reduction method [3]. The eigenvalue at the n-th step, λ^n, is determined by $\lambda^n=(\psi_0/\psi_0{}^{n-1})\lambda^{n-1}$. The iteration converges when $|\lambda^n-\lambda^{n-1}|/\lambda^n<\varepsilon_\lambda$. The value, ψ_0, is obtained by a constraint :

$$I_p = \int \lambda^n f(R,\bar{\psi}^n)dRdZ = \text{given value} \tag{13}$$

or

$$q_0 = \frac{F}{2\pi}\oint \frac{dl}{R|\nabla\psi|}\bigg|_{\bar{\psi}=0} = \text{given value} , \tag{14}$$

where I_p and q_0 denote the total plasma current and the safety factor at

the magnetic axis, respectively. This algorithm is useful when P and F are given as the function of $\bar{\psi}$.

2.3.2 Flux Conserving Tokamak (FCT) Algorithm

The Grad-Shafranov equation can be solved by specifying the profiles of the adiabatic invariant, $\mu(\bar{\psi})$, and the safety factor, $q(\bar{\psi})$, instead of $P(\bar{\psi})$ and $F(\bar{\psi})$:

$$\mu(\bar{\psi}) = P(\bar{\psi}) \left(\frac{dV}{d\chi}\right)^{\Gamma} , \tag{15}$$

and

$$q(\bar{\psi}) = \frac{1}{4\pi^2}\frac{d\chi}{d\psi} = \frac{F}{2\pi}\oint\frac{dl}{R^2 B_p} , \tag{16}$$

where χ, V and Γ are the toroidal magnetic flux, the volume surrounded by a magnetic surface and the specific heat ratio (Γ=5/3). This model describes a non-dissipative transport system and is called "Flux Conserving Tokamak (FCT)" model {4}. By substituting eq.(15) into the right hand side of the Grad-Shafranov equation (eq.(4)), we have

$$\frac{1}{R^2}\Delta^*\psi = -\mu_0 \frac{dV}{d\psi}\frac{d}{dV}\mu\left(4\pi^2 q\frac{d\psi}{dV}\right)^{\Gamma} - \frac{1}{R^2} F \frac{dF}{d\psi} . \tag{17}$$

This equation is the combination of an elliptic partial differential equation (PDE) and an ordinary differential equation (ODE). Equation (17) can be solved interatively by using the Grad-Shafranov equation and the averaged equation on a magnetic surface {5}:

$$\frac{d}{dV}\left(\langle B_p^2\rangle \frac{dV}{d\psi}\right) = -\mu_0 \frac{dP}{d\psi} - \langle R^{-2}\rangle F \frac{dF}{d\psi}, \tag{18}$$

where

$$\langle X\rangle = \lim_{\Delta V\to 0}\int_{\Delta V} X d^3x \Big/ \int_{\Delta V} d^3x = 2\pi \frac{d\psi}{dV}\oint\frac{X dl}{B_p} . \tag{19}$$

By using eqs. (15) and (16), eq.(18) is written as

$$\frac{1}{F}\frac{dF}{d\psi} = - D , \tag{20a}$$

and

$$\frac{d\chi}{dV} = F\langle R^{-2} \rangle \ , \tag{20b}$$

where

$$D = \frac{\nu\langle R^{-2}\rangle (dK/d\psi) + \mu_0 F^{\Gamma-2} (d(\langle R^{-2}\rangle^{\Gamma}\mu)/d\psi)}{\langle R^{-2}\rangle + \nu K\langle R^{-2}\rangle + \mu_0\Gamma\langle R^{-2}\rangle F^{\Gamma-2}} \ , \tag{21}$$

$$K = \nu\langle R^{-2}\rangle\langle B_p^2\rangle \cdot 2\pi \oint \frac{dl}{B_p} \ , \tag{22}$$

and

$$\nu = \frac{1}{4\pi^2 q} \tag{23}$$

The boundary condition of eq.(20) is given by

$$\chi\ (\bar{\psi}=0) = \chi(V=0) = 0 \tag{24a}$$

and

$$\chi\ (\bar{\psi}=1) = \chi\ (V=V_s) = 4\pi^2 \int_{\psi_0}^{0} q(\bar{\psi}) d\psi \ . \tag{24b}$$

The nonliner equation can be solved iteratively :

$$F^n = C \exp\left(-\int_{\psi_0}^{\psi} D(F^{n-1}) d\psi \right) \ , \tag{25}$$

and

$$\chi^n = \int_0^V F^n \langle R^{-2}\rangle dV. \tag{26}$$

The constant C is determined by the boundary condition (24b). The iteration converges when

$$| (d\chi^n/dV - d\chi^{n-1}/dV)/(d\chi^n/dV) | < \varepsilon_\chi \ . \tag{27}$$

The averaged quantities on a magnetic surface, $\langle X\rangle$, are obtained by solving the Grad-Shafranov equation (PDE) and the right hand side of PDE is obtained by using

$$F\frac{dF}{d\psi} = -F^2 D \tag{28}$$

and

$$\frac{dp}{d\psi} = \frac{d}{d\psi}\left(\mu\left(\frac{d\chi}{dV}\right)^{\Gamma}\right) . \tag{29}$$

The ODE determines $F(\psi)=RB_t$ and the toroidal magnetic field at the plasma surface, F_s, changes from the specified value (the value of the vacuum toroidal field) due to the change in the pressure. To avoid the jump of the toroidal magnetic field, the adjustment of the plasma surface is necessary such that

$$E_F(\delta r) = |\,(F^l(\bar{\psi}=1) - F_s)/F_s\,| < \varepsilon_F . \tag{30}$$

Due to the modification of the plasma surface, the vacuum magnetic field to control the plasma surface also should be corrected . The alternative iternation of PDE and ODE converges when

$$E_M = \max\{\,|\,(\psi^l(\bar{\psi})-\psi^{l-1}(\bar{\psi}))/\psi^l(\bar{\psi}))\,|\,,\,|\,(V^l(\bar{\psi})-V^{l-1}(\bar{\psi}))/V^l(\bar{\psi})\,|\ ,$$

$$|\,(\frac{dP^l}{d\psi}-\frac{dP^{l-1}}{d\psi})/\frac{dP^l}{d\psi}\,|\,,\,|\,(\frac{dF^l}{d\psi}-\frac{dF^{l-1}}{d\psi})/\frac{dF^l}{d\psi}\,|\,\}<\varepsilon_M \quad , \tag{31}$$

where l denotes the step of the iteration.

2.4 Critical pressure to the ballooning mode and local interchange mode

For a given $P(\bar{\psi})$ and $q(\bar{\psi})$, the stability of the ballooning mode and the local interchange mode are investigated. The equation of the high mode number stability is given at a magnetic surface by {6},

$$\frac{d}{dy} f(y) \frac{dG}{dy} + h(y)G = \omega^2 k(y)G , \tag{32}$$

where

$$f(y) = \frac{1}{\sqrt{g}\,|\nabla\psi|^2}\{1 + (\frac{|\nabla\psi|^2}{B}\frac{\partial z}{\partial\psi_\perp})^2\} , \tag{33}$$

$$h(y) = \frac{\sqrt{g}}{B^2}\mu_0\frac{dP}{d\psi}\frac{\partial}{\partial\psi_\perp}(2\mu_0 P + B^2) - \frac{F}{B^4}\mu_0\frac{dP}{d\psi}\frac{\partial z}{\partial\psi_\perp}\frac{\partial B^2}{\partial y}\ , \tag{34}$$

$$k(y) = \frac{1}{|\nabla\psi|^2}\{1 + (\frac{|\nabla\psi|^2}{B}\frac{\partial z}{\partial\psi_\perp})^2\}\ , \tag{35}$$

$$z(y) = \int_{y_0}^{y}\frac{\sqrt{g}F}{R^2}\,dy\ , \tag{36}$$

$$B^2 = (F^2 + |\nabla\psi|^2)/R^2\ , \tag{37}$$

$$\frac{\partial}{\partial\psi_\perp} = \frac{\nabla\psi\cdot\nabla}{|\nabla\psi|^2} \tag{38}$$

and $\sqrt{g}$ is the Jacobian. The boundary condition of eq.(32) is given by

$$G(y=-\infty) = G(y=+\infty) = 0 \tag{39}$$

When $\omega^2<0$, a ballooning mode is unstable at a magnetic surface. The marginal pressure, $dP^\infty/d\psi$, is obtained as the "eigenvalue" by solving the equation with $\omega^2=0$. The alternative iteration of the Grad-Shafranov equation and the ballooning equation with $\omega^2=0$ gives the critical pressure (the beta limit) for a given $q(\overline{\psi})$.

The asymptotic solution of eq.(32) is given by {6}

$$G(|y|\to\infty) \sim (\frac{\partial z}{\partial\psi_\perp})^\alpha\ , \tag{40}$$

where

$$\alpha = -\frac{1}{2} \pm\sqrt{1/4 - D}\ , \tag{41}$$

$$D = \frac{\mu_0(dP/d\psi)}{(4\pi^2 dq/d\psi)}\{(F^2Q_2+4\pi^2\frac{q}{F})(\mu_0\frac{dP}{d\psi}Q_3-\frac{d^2V}{d\psi^2}) + 4\pi^2\frac{dq}{d\psi}Q_1-\mu_0\frac{dP}{d\psi}F^2Q_1{}^2\}\ . \tag{42}$$

$$Q_1 = \frac{dV}{d\psi}\langle R^{-2}B_p{}^{-2}\rangle = 2\pi\oint\frac{dl}{R^2B_p{}^3}\ , \tag{43}$$

$$Q_2 = \frac{dV}{d\psi}\langle R^{-4}B_p{}^{-2}\rangle = 2\pi\oint\frac{dl}{R^4B_p{}^3}\ , \tag{44}$$

and

$$Q_3 = \frac{dV}{d\psi}\langle B_p^{-2}\rangle = 2\pi\oint \frac{dl}{B_p^3} \quad . \tag{45}$$

The condition of a non-oscillatory solution is $D<1/4$ which is the stability criterion for the local interchange mode (the Mercier criterion [7]) :

$$M = M_s + M_w + M_p > 0 \quad , \tag{46}$$

where

$$M_s = \frac{1}{4}(4\pi^2\frac{dq}{d\psi})^2 = C_1 \quad , \tag{47}$$

$$M_w = -\mu_0\frac{dP}{d\psi}C_2 = -\mu_0\frac{dP}{d\psi}\{4\pi^2\frac{dq}{d\psi}Q_1 - \frac{d^2V}{d\psi^2}(F^2Q_2 + 4\pi^2\frac{q}{F})\} \quad , \tag{48}$$

and

$$M_p = -(\mu_0\frac{dP}{d\psi})^2C_3 = -(\mu_0\frac{dP}{d\psi})^2\{F^2(Q_2Q_3-Q_1^2) + 4\pi^2\frac{q}{F}Q_3\} \quad . \tag{49}$$

The ballooning equation with $\omega^2=0$ is solved in a bounded domain of y, $[0,2\pi N]$, assuming $y_0=0$ for a up-and-down symmetric case , where N is the numbers of turns in the integration of the equation. The marginal equation is solved numerically by using the Runge-Kutta Method or the matrix method with the boundary conditions

$$G(0) = \text{finite} \quad , \tag{50}$$

and

$$G(2\pi N) = 0 \quad . \tag{51}$$

When the Mercier criterion is violated, the marginal equation has the oscillatory solution and the boundary condition (51) can not be used. In this case, the marginal pressure $dP^\infty/d\psi$ is obtained by using the criterion of the local interchange mode:

$$\mu_0 dP^\infty/d\psi = -(C_2 + \sqrt{C_2^2+4C_1C_3})/(2C_3) \quad . \tag{52}$$

2.5 Data set for benchmark calculation

2.5.1 Definition of Parameters

In this section, the basic parameters used in the equilibrium calculation are summarized

(1) Geometrical parameters (Fig.2)

Aspect ratio : $A = R_0/a$ (53)

Ellipticity : $\kappa = b/a$ (54)

Triangularity : $\delta = \triangle/a$ (55)

(2) Physical parameters

Flux safety factor : $q = \frac{F}{2\pi}\oint_\psi \frac{dl}{R\,|\nabla\psi|}$ (56)

Current safety factor : $q_{J1} = \frac{5\bar{a}^2 B_{t0}}{R_0 I_p\,(MA)}$ (57)

$(\bar{a}=\sqrt{D/\pi}$, D : Area of cross section)

$$q_{J2} = \frac{5\kappa a^2 B_{t0}}{R_0 I_p\,(MA)} \quad (58)$$

$$q_{J3} = \frac{5k a^2 B_{t0}}{R_0 I_p\,(MA)} \quad (59)$$

$(k=(1+\kappa^2)/2)$

where B_{t0} is the vacuum toroidal magnetic field at $R=R_0$ and $Z=0$.

Beta value : $B_t = 2\mu_0\bar{P}/B_{t0}^2 \quad (\bar{P} = \int P d^3x / \int d^3x)$ (60)

Poloidal beta value : $\beta_J = 4\mu_0 \int P d^3x / [R_0\{\mu_0 I_p(A)\}^2]$ (61)

$$\beta_p = \frac{2\mu_0 \overline{P}}{\hat{B}_p^2} \quad \left(\hat{B}_p = \frac{\mu_0 I_p(A)}{\oint_{\psi=1} dl}\right) \tag{62}$$

Shear : $S = \frac{2V}{q}\frac{dq}{dV}$ $\left(= \frac{\rho}{q}\frac{dq}{d\rho} \; ; \rho = \sqrt{V/2\pi^2 R_0}\right)$ (63)

Local poloidal beta value : $\alpha = -\frac{\mu_0}{2\pi^2}\frac{dP}{d\psi}\frac{dV}{d\psi}\sqrt{V/2\pi^2 R_0}$

$$\left(= -\rho^2 R_0 \mu_0 \frac{dP}{d\rho} \Big/ \left(\frac{1}{R_0}\frac{d\psi}{d\rho}\right)^2\right) \tag{64}$$

Averaged parallel current :

$$I_{\parallel} = \frac{\langle J \cdot B \rangle}{\langle B^2 \rangle} = -\frac{F}{\langle B^2 \rangle}\frac{dP}{d\psi} - \frac{1}{\mu_0}\frac{dF}{d\psi} \tag{65}$$

2.5.2 Descriptions on Equilibrium Code

In Tables 1 and 2, numerical methods and parameters used in the equilibrium code are summarized.

Table 1 Procedure and numerical method

Procedure	Numerical method
Plasma shape	6 points fitting in eq. (5). $\theta = 0, \pi, 0.5\pi \pm 0.15, 0.25\pi, 0.35\pi$
Trace of contour	Liner interpolation in (R,Z) plane
Interpolation & derivative	Cubic spline function
Numerical integration	Trapezoidal rule
PDE	Double cyclic reduction
ODE	Trapezoidal rule

Table 2 Parameters of numerical calculation

Variable	Contents	Value
NR	Mesh points in R	257
NZ	Mesh points in Z	129
NV	Numbers of contours	101
N	Numbers of turns in ballooning equation	10
ε_λ	Convergence in Nonlinear eigenvalue problem	10^{-3}
ε_χ	Convergence in ODE	10^{-5}
ε_F	Convergence in volume control	10^{-4}
ε_M	Convergence in FCT calculation	10^{-3}

2.6 Example of equilibrium

For the stability calculation, we use four kinds of up-and-down symmetric equilibria with A=4, R_0=4, a=1, κ=1.6, δ'=0.3 ($\delta\sim$0.3), q_0=1.1 and $q_a\sim$3.1 and 3.2 . The profile of the safety factor is obtained by using the algorithm of the nonlinear eigenvalue problem with the following profiles of $dP/d\psi$ and $F(dF/d\psi)$:

$$\frac{dP}{d\psi}(\bar{\psi}) = \beta_l (1 - \bar{\psi}^{i1})^{i2} \tag{66}$$

and

$$F\frac{dF}{d\bar{\psi}}(\bar{\psi}) == R_0^2\left(\frac{1}{\beta_l} - 1\right)\mu_0\frac{dP}{d\bar{\psi}}(\bar{\psi}) \ . \tag{67}$$

The vacuum toroidal magnetic field is chosen as B_{t0}=5.5 at the center of the horizontal midplane. By fixing $q(\bar{\psi})$ obtained from the profile (66) and (67) with β_l=0.001, the pressure is increased in FCT sequence. Table 3 shows the parameters $(j1, j2)$ and the profile of $P(\bar{\psi})$ in the FCT sequence.

Table 3 (j1, j2) and pressure profile

	Data 1	Data 2	Data 3	Data 4
(j_1, j_2)	(2.3, 2.0)	(2.3, 2.0)	(1.15, 1.0)	(1.15, 1.0)
q_0	1.1	1.1	1.1	1.1
Calculated q_a	3.12	3.12	3.20	3.20
Pressure	P1	P2	P2	P3 (x_0 = 0.95)

P1 : $P(\bar{\psi}) = P_0(1 - 0.2\bar{\psi} - 2.6\bar{\psi}^2 + 1.8\bar{\psi}^3)$

P2 : The marginal pressure, $P(\bar{\psi})^{\infty} = -\int_{\psi_0}^{0} (dP^{\infty}/d\psi)d\psi$, to the ballooning mode.

P3 : The marginal pressure with the form factor, $S(\bar{\psi}) = 2/\{1+\exp(\bar{\psi}/x_0)^{32}\}$.

The pressure is increased by using the profiles shown in Table 3 with the increment of $\Delta\beta \sim 0.2$ % . In the cases of P2 and P3, the increment of the pressure is given by using the marginal pressure profile of the former step :

$$P^{n-1} \rightarrow (\psi^{n-1}, \beta^{n-1}) \rightarrow (P^{\infty,n-1}, \beta^{\infty,n-1}) \rightarrow P^n, \tag{68}$$

$$P^n(\bar{\psi}) = C_P\, P^{\infty,n-1}(\bar{\psi}) \ , \tag{69}$$

and

$$C_P = \frac{\beta^{n-1} + \triangle\beta}{\beta^{\infty,n-1}} \ . \tag{70}$$

This procedure is not a complete optimization with respect to the ballooning mode but the FCT sequence by using the nearly marginal profile of the pressure. The iteration with C_P=1 in eq.(69) gives the optimized beta limit for a given q-profile. In Fig.3 to Fig.6 (which correspond to from Data 1 to Data 4, respectively), subfigures (a)-(j) show the following quantities:

(a) Contour of equi-ψ. The symbol, *, denotes the position of a null point.

(b) Contour of equi-J_φ.

(c) Plasma pressure, $P(R,Z=0)$.

(d) Safety factor, $q(R,Z=0)$.

(e) Toroidal current density, $J_\varphi(R,Z=0)$.

(f) Safety factor, $q(\bar{\psi})$.

(g) Pressure gradient $dP/d\psi$. The broken line shows the marginal pressure gradient, $dP^\infty/d\psi$.

(h) Diamagnetic current density, $F(dF/d\psi)$.

(i) Averaged parallel current density.

(j) Stability diagram in S-α plane. The right side of the curve is a stable region of the ballooning mode. The broken line denotes the marginal line obtained by using $dP^\infty/d\psi$.

These figures show the quantities at the nearly beta limit due to the ballooning mode. In Table 4, the beta limit due to the ballooning mode and other quantities are summarized.

For Data 1 and 2, the shear is weak near the magnetic axis and the numbers of turns for the integration of the ballooning equation should be increased. In the present calculation, the marginal pressure is

obtained by using eq. (52), when the Mercier criterion is violated. However, it does not affect the beta limit too much because of a small volume of this region.

Table 4 Beta limits and other related quantities.

	Data 1	Data 2	Data 3	Data 4
β_B (%)	3.0	4.3	4.1	3.5
β_J	1.2	1.6	1.7	1.5
I_p (MA)	5.5	5.6	5.4	5.3
g_B (%)	3.0	4.2	4.2	3.7
q_{J1}	1.97	1.92	2.02	2.04

3. Stability calculation

In this section, the ideal MHD stability of the n=1 external kink mode is studied for the four cases of equilibria described in §2.

3.1 Basic equation

The stability of the ideal MHD modes is studies by minimizing a Lagrangean {8},

$$L = W_P + W_V - \omega^2 W_K \ , \tag{71}$$

$$W_p = \frac{1}{2}\int_P d^3x \, [\, |\, Q + (n\cdot\xi)(J_0\times n)\,|^2 + \Gamma P_0 |\, \nabla\cdot\xi\,|^2 - 2\,|\, n\cdot\xi\,|^2 (J_0\times n)\cdot(B_0\cdot\nabla)n\,] \quad , Q = \nabla\times(\xi\times B_0) \tag{72}$$

$$W_V = \frac{1}{2}\int_V d^3x \,|\, \nabla\times A\,|^2 \ , \tag{73}$$

and

$$W_K = \frac{1}{2}\int_P d^3x \rho_0 \,|\, \xi\,|^2 \ . \tag{74}$$

Here ξ is the displacement of the fluid element, n is the unit vector normal to the equilbrium magnetic surface ($n=\nabla\psi/|\nabla\psi|$), and ρ_0 is the mass density. The quantities with a subscript 0 denote ones in an equilibrium. The perturbation of the vacuum energy in eq.(73) is given by using the vector potential, A, and the boundary conditions for ξ and A are given by {8}

$$n\times A = -(n\cdot\xi)B_0 \quad \text{at the plasma surface} \ , \tag{75}$$

and

$$n\times A = 0 \quad \text{at the conducting shell or infinity.} \tag{76}$$

The potential energy of the plasma motion, eq.(72), can be written in

the other form [9],

$$W_p = \frac{1}{2}\int d^3x \left[\left| Q - \frac{\xi \cdot \nabla P_0}{B_0^2} B_0 \right|^2 - \frac{J_0 \cdot B_0}{B_0^2} \xi \times B_0 \cdot Q + \Gamma P_0 |\nabla \cdot \xi|^2 \right.$$

$$\left. - 2\xi \cdot \nabla P_0 \xi \cdot \kappa_0 \right] , \tag{77}$$

where

$$\kappa_0 = \frac{B_0 \times [B_0 \times \nabla (2P_0 + B_0^2)] \times B_0}{2B_0^2} . \tag{78}$$

This form is used in the analysis of the driving mechanism of the instability. The first term in eq.(77) works as the stabilizing term due to the bending and the compression of a magnetic field. The second term and the fourth term are the destabilizing terms due to the current and the pressure gradient and they are called the kink and the ballooing terms, respectively. The weakly unstable MHD modes localize near the rational surface where $q(\psi)$ takes a rational number. For the accurate calculation of the eigenvalue, ω^2 , and the eigenvector, it is necessary to use a flux surface coordinate, (ψ, χ, φ), where χ is the azimuthal coordinate. In the axisymmetric system, the equilibrium quanties are independent of φ and the Largangean can be written in the form of the single summation with respect to the toroidal mode number, n,

$$L = \sum_n L_n , \tag{79}$$

and

$$\xi(\psi, \chi, \Phi) = \sum_n \xi_n(\psi, \chi) e^{in\varphi} . \tag{80}$$

The Fourier-component, $\xi_n(\psi, \chi)$, is written in the contravarient form :

$$\xi_n = R^2 X (\nabla\chi \times \nabla\varphi) + R^2 V \nabla\varphi \times \nabla\psi + R^2 Y B_0 . \tag{81}$$

3.2 Numerical method

The details of the numerical methods of the stability code, ERATO, is described in Ref.[10]. Here, one of the most important procedures in the ERATO-J code is described, i.e. the mapping from the (R,Z,φ) coordinate to the flux coordinate, (ψ,χ,φ). The azimuthal coordinate, χ, is defined by

$$\chi = \int_0^l \frac{dl}{\sqrt{g}B_p} \text{ with } 2\pi = \oint_\psi \frac{dl}{\sqrt{g}B_p} , \tag{82}$$

where $\sqrt{g}$ is the Jacobian of the flux coordinate system. One of the typical coordinate systems is given by

$$\sqrt{g} = \frac{qR^2}{F} . \tag{83}$$

In this coordinate system, the angle between the toroidal and poloidal magnetic field lines is constant on a magnetic surface:

$$\frac{B^\varphi}{B^\chi} = \frac{\sqrt{g}F}{R^2} = q(\psi) , \tag{84}$$

Where B^φ and B^χ are the contravarient components of the magnetic field. This coordinate system is called "a natural coordinate system".

For the mapping, the trace of the magnetic surface and the numerical derivatives with the high accuracy are inevitable. In the ERATO-J code, the 3rd order or the 5th order spline interpolation is used in the (R,Z) space. The magnetic surface is traced by solving the equation of the magnetic field line:

$$\frac{dR}{dl} = \frac{1}{|\nabla\psi|}\frac{\partial\psi}{\partial Z} , \quad \frac{dZ}{dl} = -\frac{1}{|\nabla\psi|}\frac{\partial\psi}{\partial R} , \tag{85}$$

where dl is the element of the arc length along the magnetic surface. The differential equations (85) are solved by using the 4th order Runge-Kutta method. Along the magnetic surface, the derivatives of $\psi(R,Z)$ are calculated by using the two dimentional spline function. Figure 7 shows the convergence of the squared growth rate, $\gamma^2=-\omega^2/\omega_A{}^2$, with respect to the mesh size, N_ψ, and N_χ, where $\omega_A{}^2=F_0{}^2/(\mu_0\rho_0R_0{}^4)$ and $F_0=F(\bar{\psi}=0)$. The broken line denotes the case of the linear

interpolation and the finite difference approximation of the derivatives. This approximation does not give the quadratic convergence of γ^2 with respect to mesh size. The 3rd order interpolation as well as the trace by using the Runge-kutta method gives the quadratic convergence (the solid line).

The mesh accumlation is efficient to describe the ideal MHD modes near the beta limit. In the ERATO-J code, the weight of the mesh accumlation is given by

$$\frac{dW}{ds} = 1+\sum_i \frac{C_i}{1+[(s-s_i)^2/W_i]^2} , \tag{86}$$

where $s=\sqrt{\bar{\psi}}$. The mesh point in s is obtained by $W_j=W(s_j)$ (W_j: equi-distant mesh in W space).

3.3 Data set for benchmark calculation

In Table 5, the parameters used in the stability analysis are shown.

Table 5 Data set for ERATO-J

Parameter	Contents	Value
-	Coorinate	Natural in χ $s=\sqrt{\bar{\psi}}$
N_{ψ}	mesh numbers in s	101
N_{χ}	mesh numbers in χ (only upper half plane)	81
C_1	eq. (86)	1.0
W_1	eq. (86)	0.1
s_1	eq. (86)	0.9
ε_{ω}	Convergence of ω^2 in the eigenvalue solver	10^{-4}
n	Toroidal mode number	1
R_{wall}	Position of Conducting Wall	∞

3.4 Growth rate and beta limit

The stability of the n=1 external kink mode is studied for the four classes of equilibria (Data 1 - Data 4) described in §2.6. Figure 8 shows the squared growth rate, $\gamma^2=-\omega^2/\omega_A{}^2$, as the function of β_t for the Data 1. The beta limit is $\beta_K\sim3.8\%$. Figs. 9-11 shows (a) the safety factor as the function of $s=\sqrt{\bar{\psi}}$, (b) the eigenmode $X(s,\chi=0)$, (c) the eigenmode $V(s,\chi=0)$ and (d) driving terms averaged on a magnetic surface. The symbols A, K and B denote the bending of the magnetic field, the kink term and the ballooning term given in eq. (77),

respectively. In Table 6, the growth rate and the beta value are summarized for Data 1.

Table 6 Squared growth rate and β_t for Data 1

β_t (%)	γ^2	β_J	I_p (MA)	q_{J1}	mode
4.80	3.28×10^{-3}	1.77	5.68	1.90	Fig.11
4.60	1.92×10^{-3}	1.71	5.66	1.91	
4.40	9.99×10^{-4}	1.65	5.63	1.92	
4.20	4.21×10^{-4}	1.59	5.60	1.92	
4.00	1.16×10^{-4}	1.52	5.58	1.93	Fig.10
3.80	1.45×10^{-5}	1.46	5.55	1.94	Fig.9

The operator in the ERATO code has a branch of a continuum spectrum in the vicinity of $\omega^2=0$. The eigenfunction of the continuum spectrum has the singularity at a rational surface. Due to the discrete space in $\bar{\psi}$ and χ, the continuum spectrum appears in the unstable side by a numerical reason. Therefore ,when the sharp peak in the eignmode, V, localizes with a few meshes, a plasma is considered to be marginally stable. Figs.9 (c) and (d) show the structure for a nearly marginal state. The growth rate is $\gamma^2=-\omega^2/\omega_A^2=1.45\times10^{-5}$. This result indicates the σ-stability criterion [11] with $\sigma^2=1.0\times10^{-5}$. For Data 2, 3 and 4, the squared growth rates and the beta values are shown in Tables 7, 8 and 9, respectively. The mode structures near the beta limit are also shown in Figs.12 to 17. The beta limits due to the ballooning mode and the kink mode are summarized in Table 10.

Table 7 Growth rate and β_t for Data 2

β_t (%)	γ^2	β_J	I_p (MA)	q_{J1}	mode
4.70	2.78×10^{-4}	1.75	5.66	1.91	
4.50	8.13×10^{-5}	1.69	5.63	1.92	
4.31	2.24×10^{-5}	1.63	5.61	1.92	Fig.13
4.12	8.91×10^{-6}	1.57	5.59	1.93	Fig.12

Table 8 Growth rate and β_t for Data 3

β_t (%)	γ^2	β_J	I_p (MA)	q_{J1}	mode
3.92	8.06×10^{-4}	1.64	5.33	2.02	
3.73	2.91×10^{-4}	1.57	5.30	2.03	
3.53	4.24×10^{-5}	1.50	5.28	2.04	Fig.15
3.34	4.06×10^{-6}	1.44	5.25	2.05	Fig.14

Table 9 Growth rate and β_t for Data 4

β_t (%)	γ^2	β_J	I_p (MA)	q_{J1}	mode
3.72	8.06×10^{-4}	1.57	5.38	2.03	
3.53	2.91×10^{-4}	1.50	5.28	2.04	
3.34	4.53×10^{-5}	1.43	5.25	2.05	Fig.17
3.14	9.45×10^{-6}	1.36	5.23	2.06	Fig.16

Table 10 Beta limit due to ballooning mode and kink mode

Data	β_B (%)	g_B (%)	β_K (%)	g_K (%)
Data 1	3.0	3.0	3.8	3.8
Data 2	4.3	4.2	4.2	4.1
Data 3	4.1	4.2	3.4	3.5
Data 4	3.5	3.7	3.2	3.4

4. Summary

In this report, we described the basic equations and the numerical methods for the analysis of the ideal MHD beta limit of a tokamak plasma. We also propose the data set for the benchmark calculation on the beta limit of INTOR plasma. We chose four classes of equilibria. In Data 1 and Data 2, the shear is weak near the magnetic axis and is strong near the plasma surface. In Data 1, the pressure is increased by fixing the profile which is close to the optimized one near the

Table 9 Growth rate and β_t for Data 4

β_t (%)	γ^2	β_J	I_p (MA)	q_{J1}	mode
3.72	8.06×10^{-4}	1.57	5.38	2.03	
3.53	2.91×10^{-4}	1.50	5.28	2.04	
3.34	4.53×10^{-5}	1.43	5.25	2.05	Fig.17
3.14	9.45×10^{-6}	1.36	5.23	2.06	Fig.16

Table 10 Beta limit due to ballooning mode and kink mode

Data	β_B (%)	g_B (%)	β_K (%)	g_K (%)
Data 1	3.0	3.0	3.8	3.8
Data 2	4.3	4.2	4.2	4.1
Data 3	4.1	4.2	3.4	3.5
Data 4	3.5	3.7	3.2	3.4

4. Summary

In this report, we described the basic equations and the numerical methods for the analysis of the ideal MHD beta limit of a tokamak plasma. We also propose the data set for the benchmark calculation on the beta limit of INTOR plasma. We chose four classes of equilibria. In Data 1 and Data 2, the shear is weak near the magnetic axis and is strong near the plasma surface. In Data 1, the pressure is increased by fixing the profile which is close to the optimized one near the

magnetic axis. The kink limit is greater than the ballooning limit. In Data 2, the pressure is increased by using the marginal pressure at each iteration step. The two limits coincide with each other. In this case the toroidal current density has a finite value at the plasma surface, but the averaged parallel current density is small. For Data 3, the kink limit is smaller than the ballooning limit mainly due to the weaker shear near the plasma surface. By the reduction of the pressure gradient near the plasma surface, two limits become closer. For the data base assessment in the international collaboration, it is necessary to compare the results in wider range of parameters and to summarize them from the physical point of view.

Acknowledgement

This work is based on the discussion at the 13th session of INTOR workshop, Phase Two A, Part III (Group B) with Drs. F. Engelmann, A. Knobloch (EC), Y. -K. Peng (USA), Y.L. Igitkhanov and R. N. Litunovskij (USSR). The authors express their sincere thanks to the members of the Group B of the INTOR workshop for the excellent guidance and helpful discussions on this work. The authors greatly appreciate Dr. M. Tanaka's continuous encouragements.

References

{1} INTOR Phase Two A Part II (IAEA, Vienna) (1986) 453.
{2} F. Troyon et al., Plasma Phys. 26 (1984) 209.
{3} R. W. Hockney, *Method in Computational Physics* Vol.9 (Academic Press, New York) (1970) 135.
{4} J. F. Clarke and D. J. Sigmar, Phys. Rev. Lett. 38 (1977) 70.
{5} H. Grad et al., Proc. Nat. Acad. Sci. (USA) 72 (1975) 3789.
{6} J. W. Connor et al., Proc. Roy. Soc. (London) A365 (1979) 1.

[7] C. Mercier, Nucl. Fusion 1 (1960) 47.
Y. -K. M Peng et al., Phys. Fluids 21 (1978)
[8] I. B. Bernstein et al., Proc. Roy. Soc. (London) 244 (1958) 17.
[9] J. M. Greene and J. L. Johnson, Plasma Phys. 10 (1968) 729.
[10] R. Gruber et al., Comput. Phys. Commum. 21 (1981) 323.
[11] P. H. Sakanaka and J.P. Goedbloed, Phys. Fluids 17 (1974) 919.

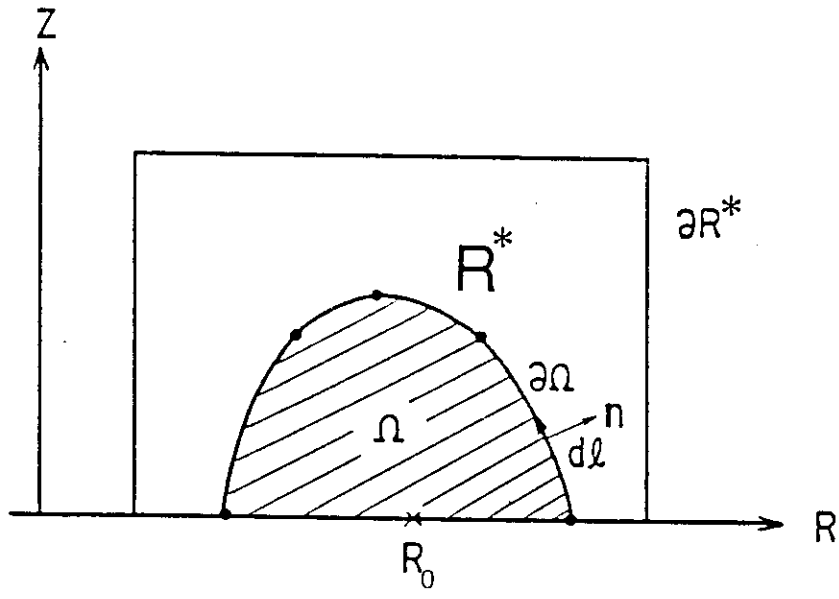

Fig.1 Rectangular domain for Grad-Shafranov equation. Boundary condition is given on ∂R^*

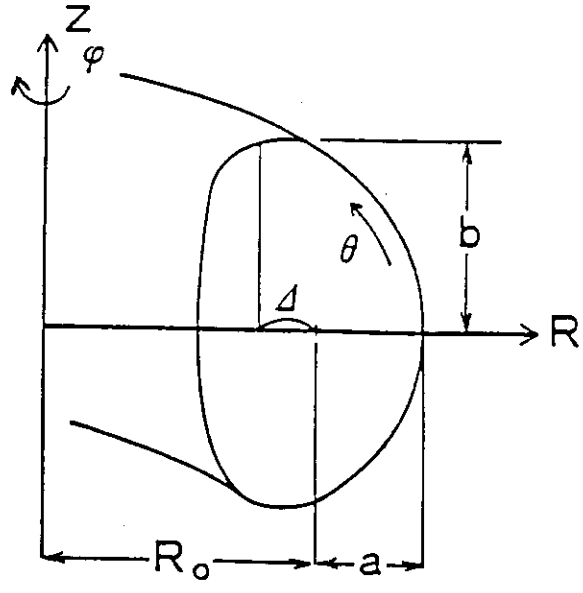

Fig.2 Definition of geometrical parameters.

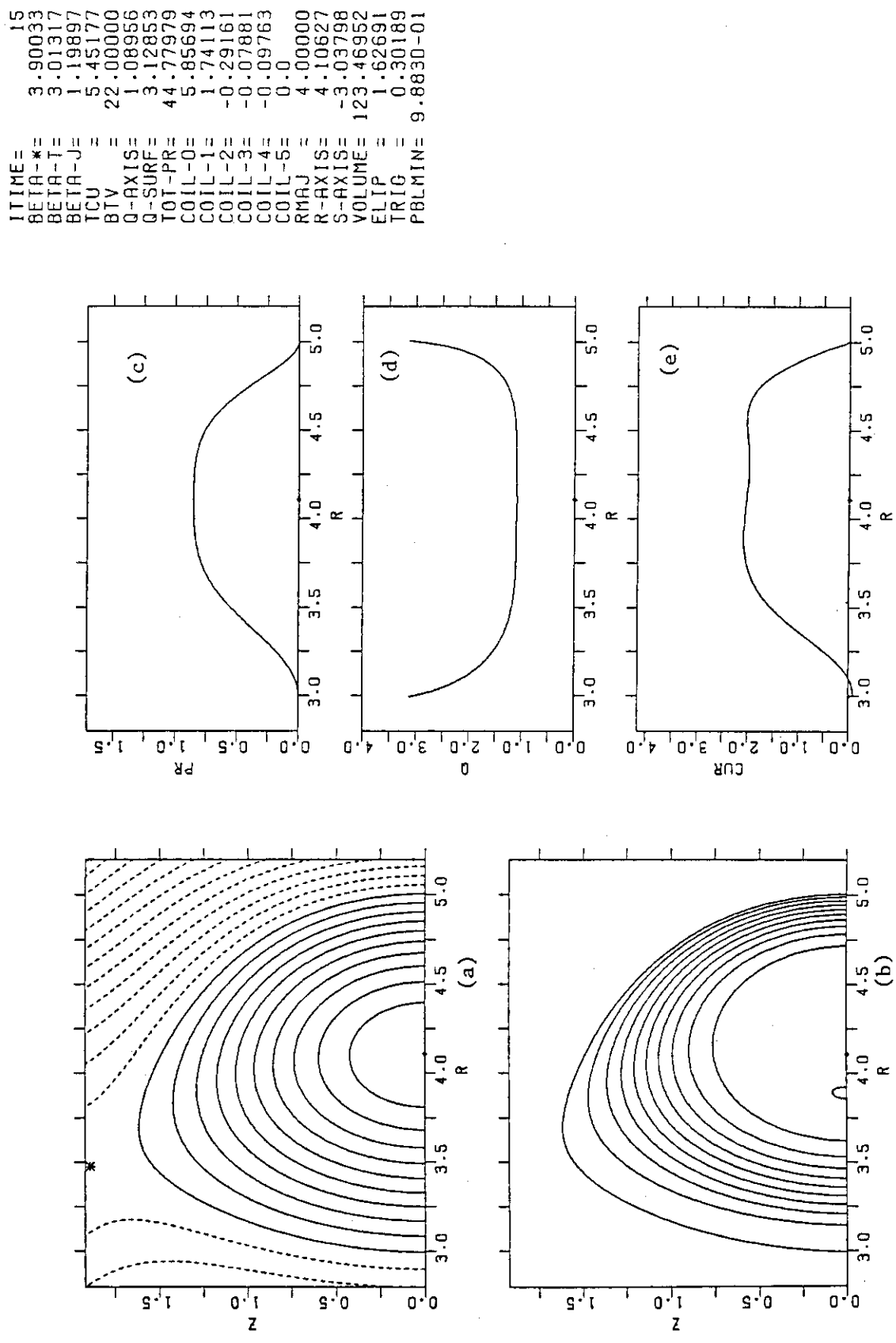

Fig.3 Profiles in equilibrium Data 1. β_t=3.01%.

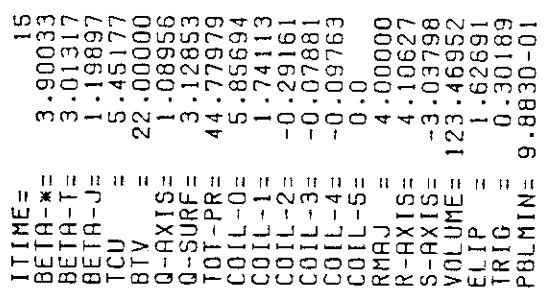

Fig.3 Profiles in equilibrium Data 1. β_t=3.01%.

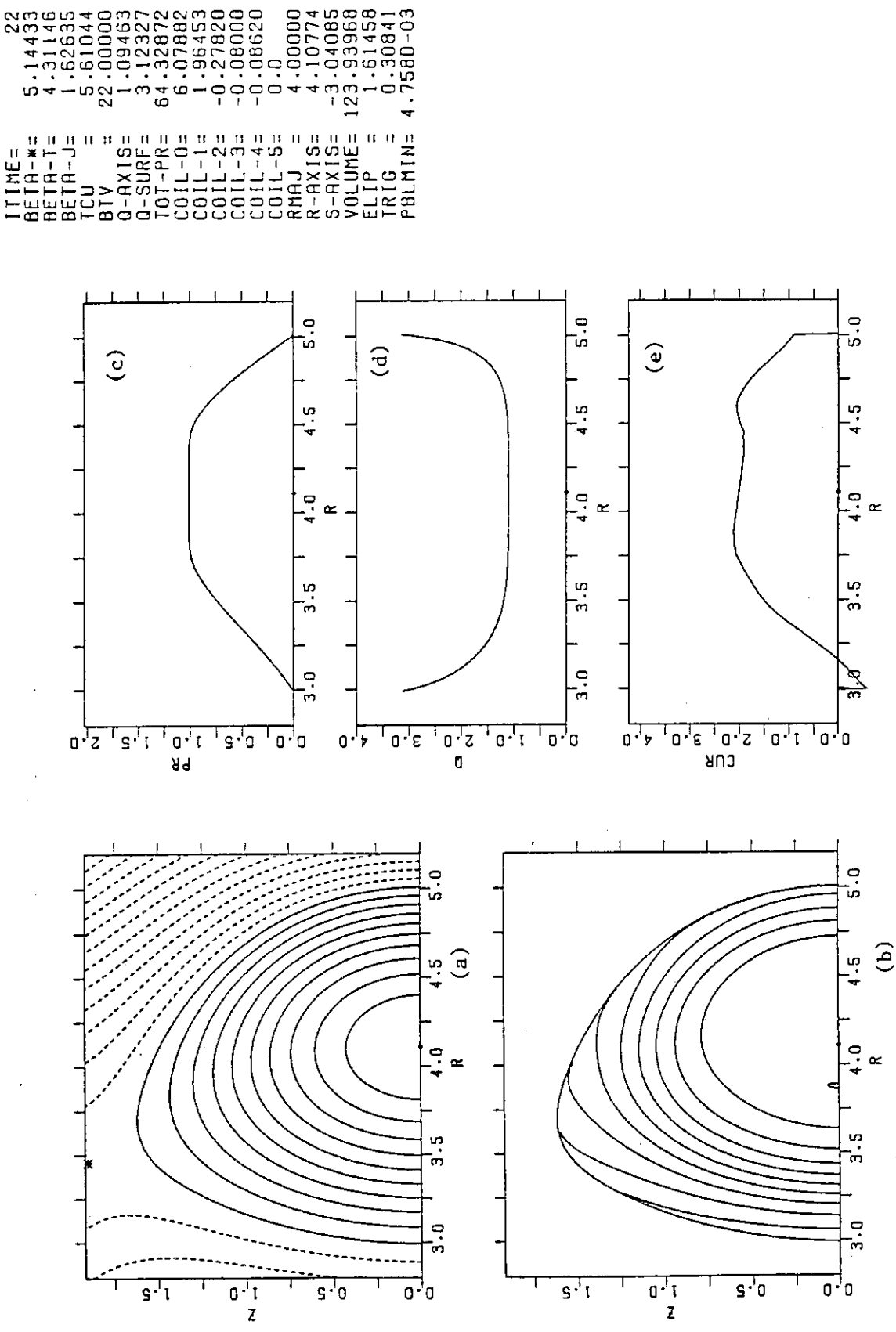

Fig.4 Profiles in equilibrium Data 2. β_t=4.31%.

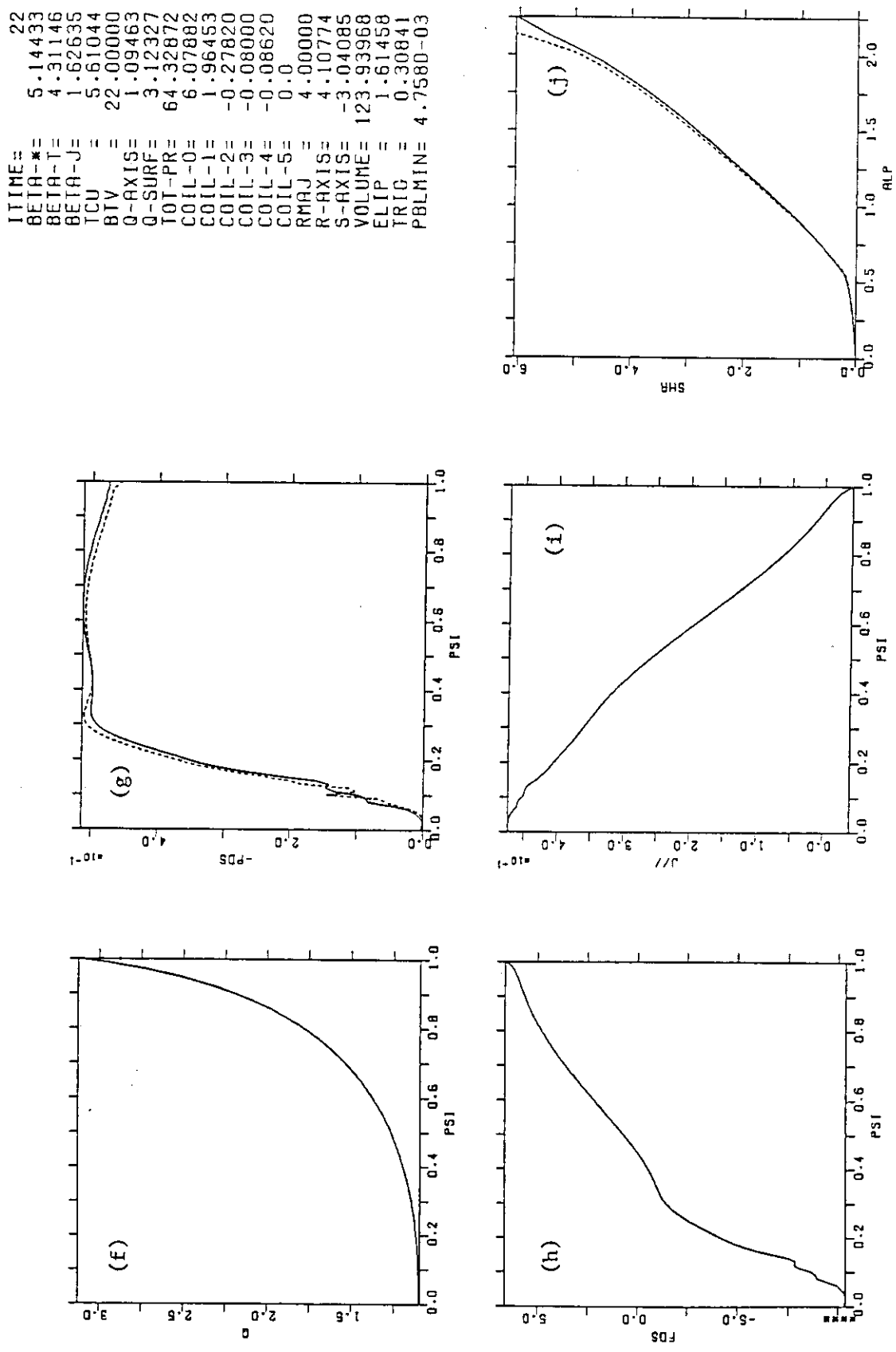

Fig.4 Profiles in equilibrium Data 2. β_t=4.31%.

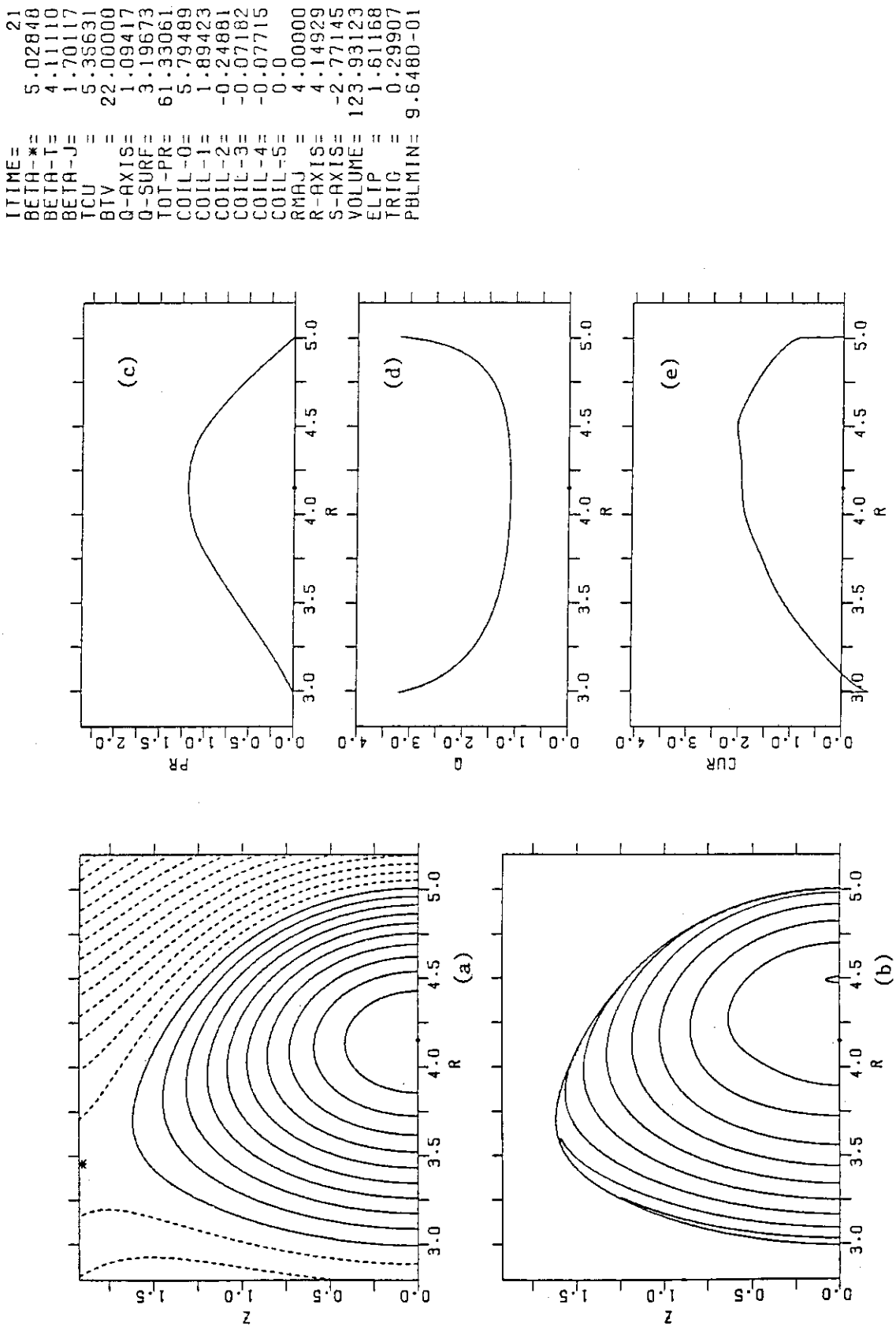

Fig.5 Profiles in equilibrium Data 3. β_t=4.11%.

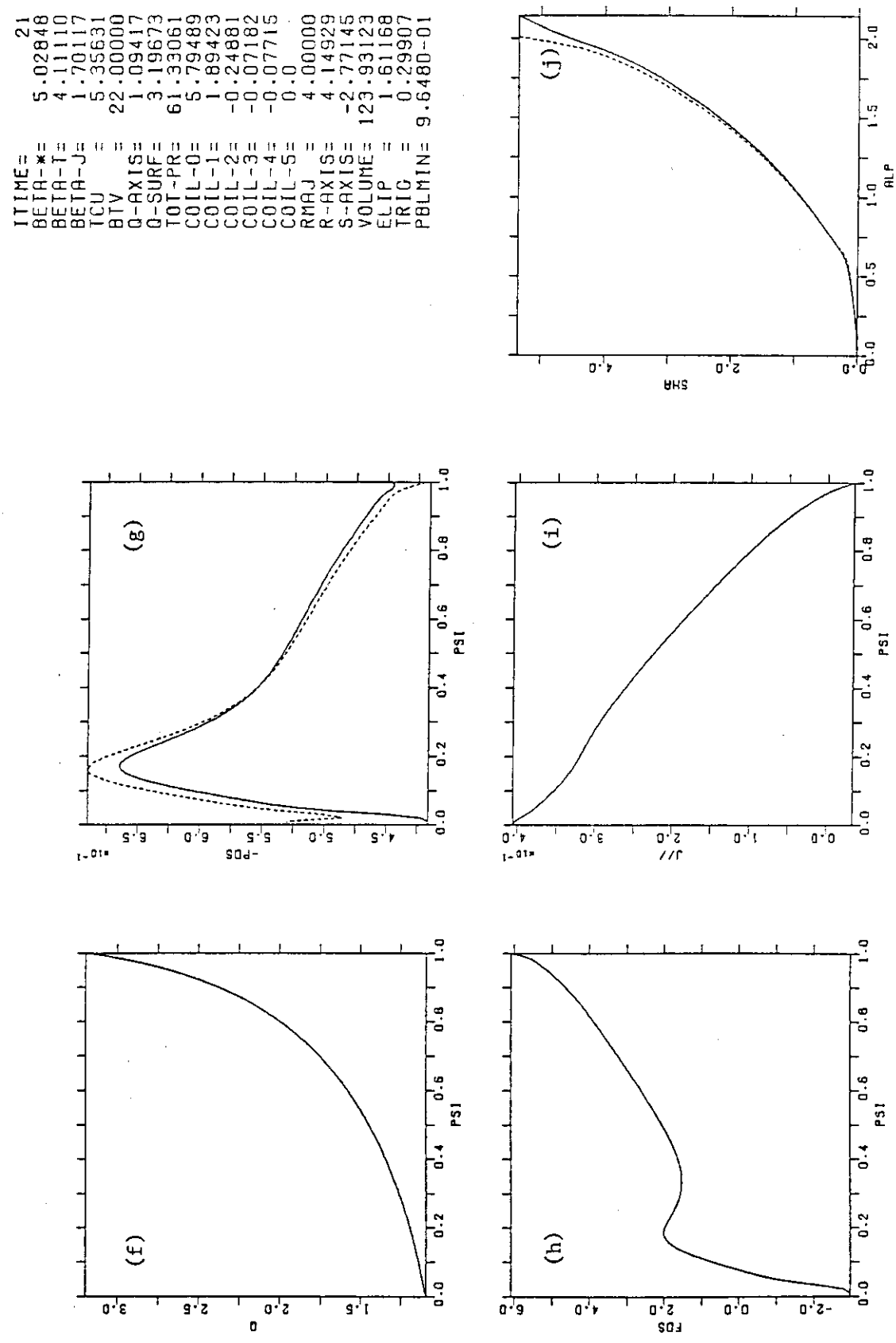

Fig.5 Profiles in equilibrium Data 3. β_t=4.11%.

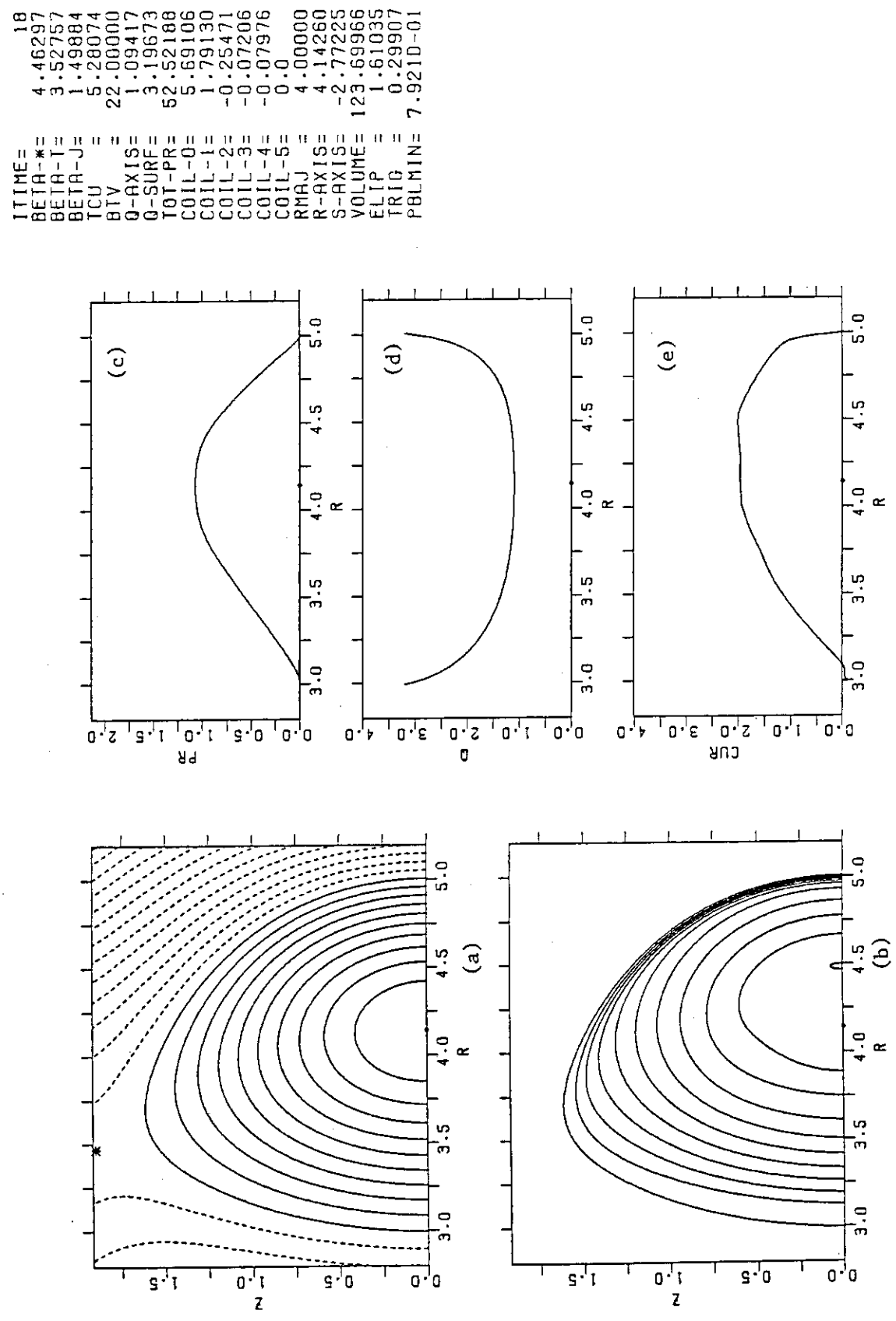

Fig.6 Profiles in equilibrium Data 4. β_t=3.53%.

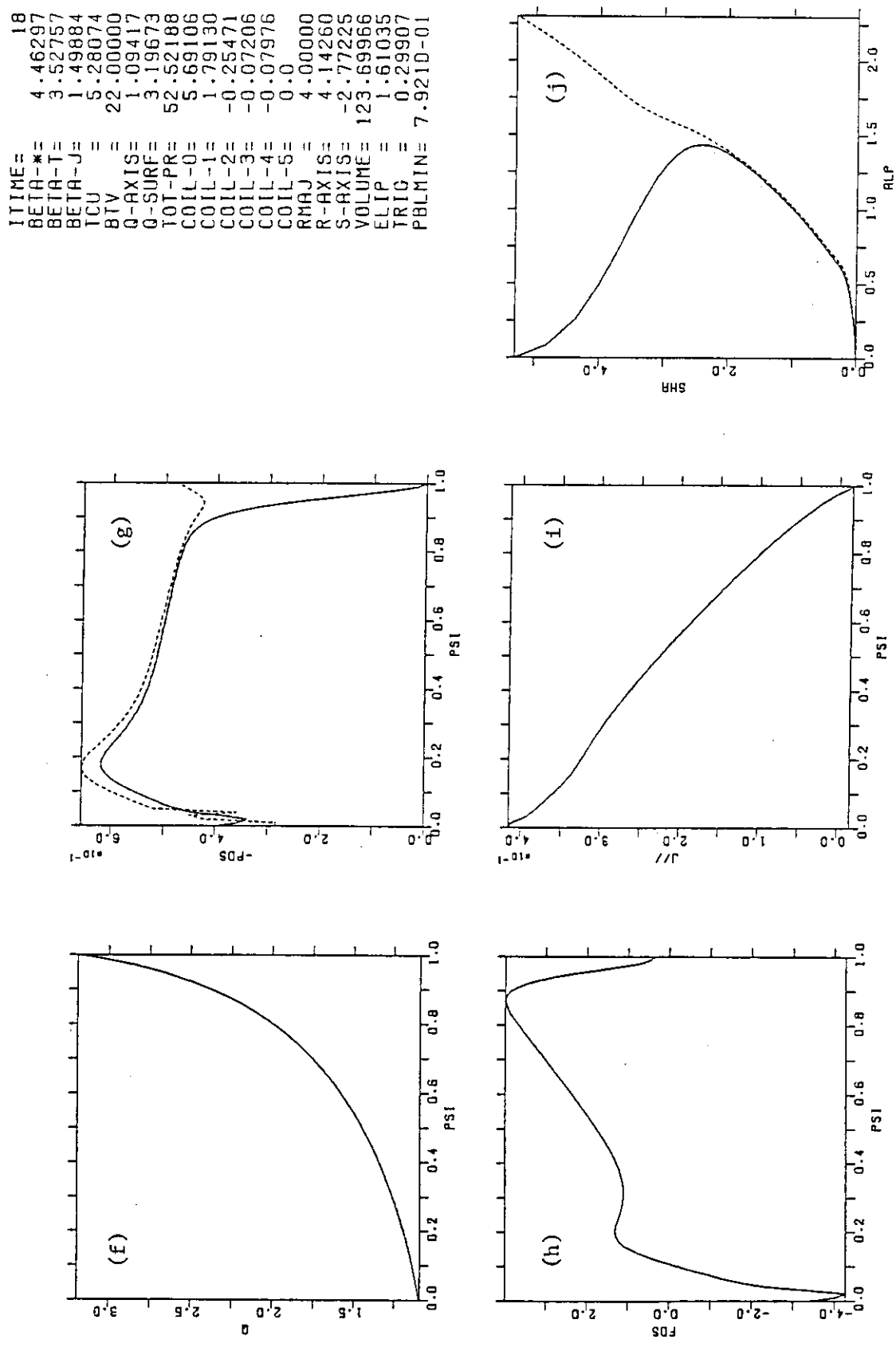

Fig.6 Profiles in equilibrium Data 4. β_t=3.53%.

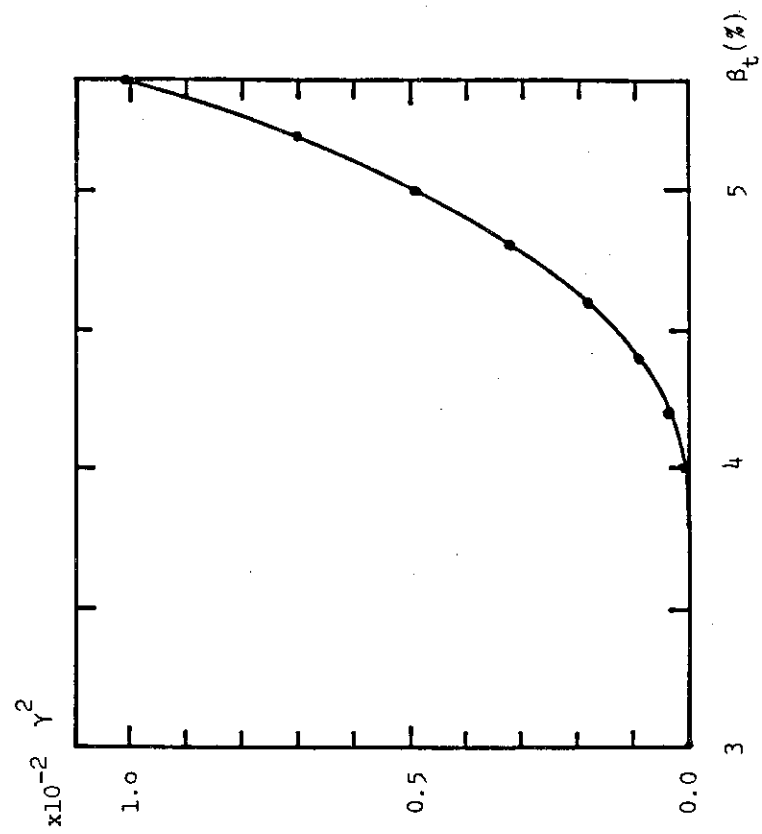

Fig.8 Squared growth rate vs. β_t for the equilibrium Data 1.

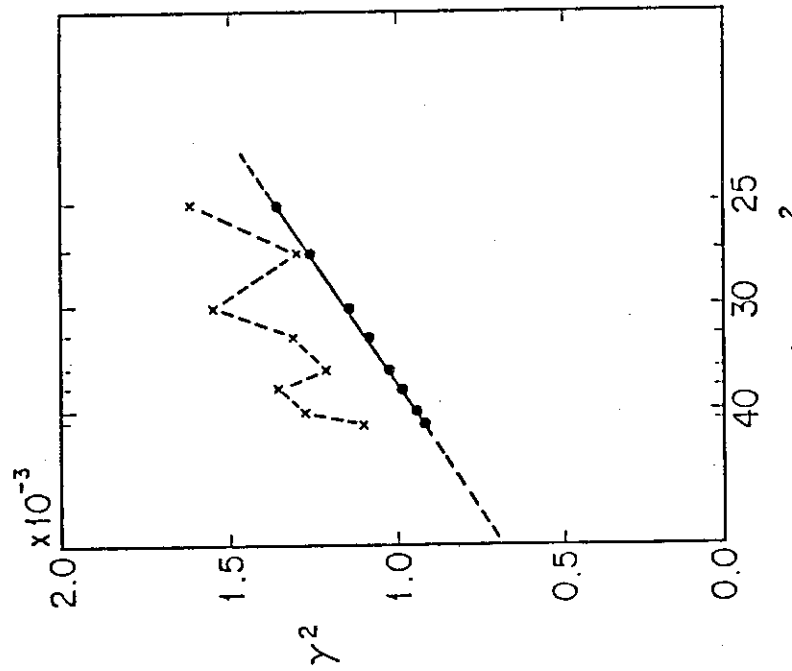

Fig.7 Eigenvalue vs. mesh numbers $N=N_\psi=N_\chi$.
Broken line denotes the case of a linear interpolation and a finite difference method.
Quadratic convergence with respect to $1/N$ is shown by using the 3rd order spline interpolation (solid line).

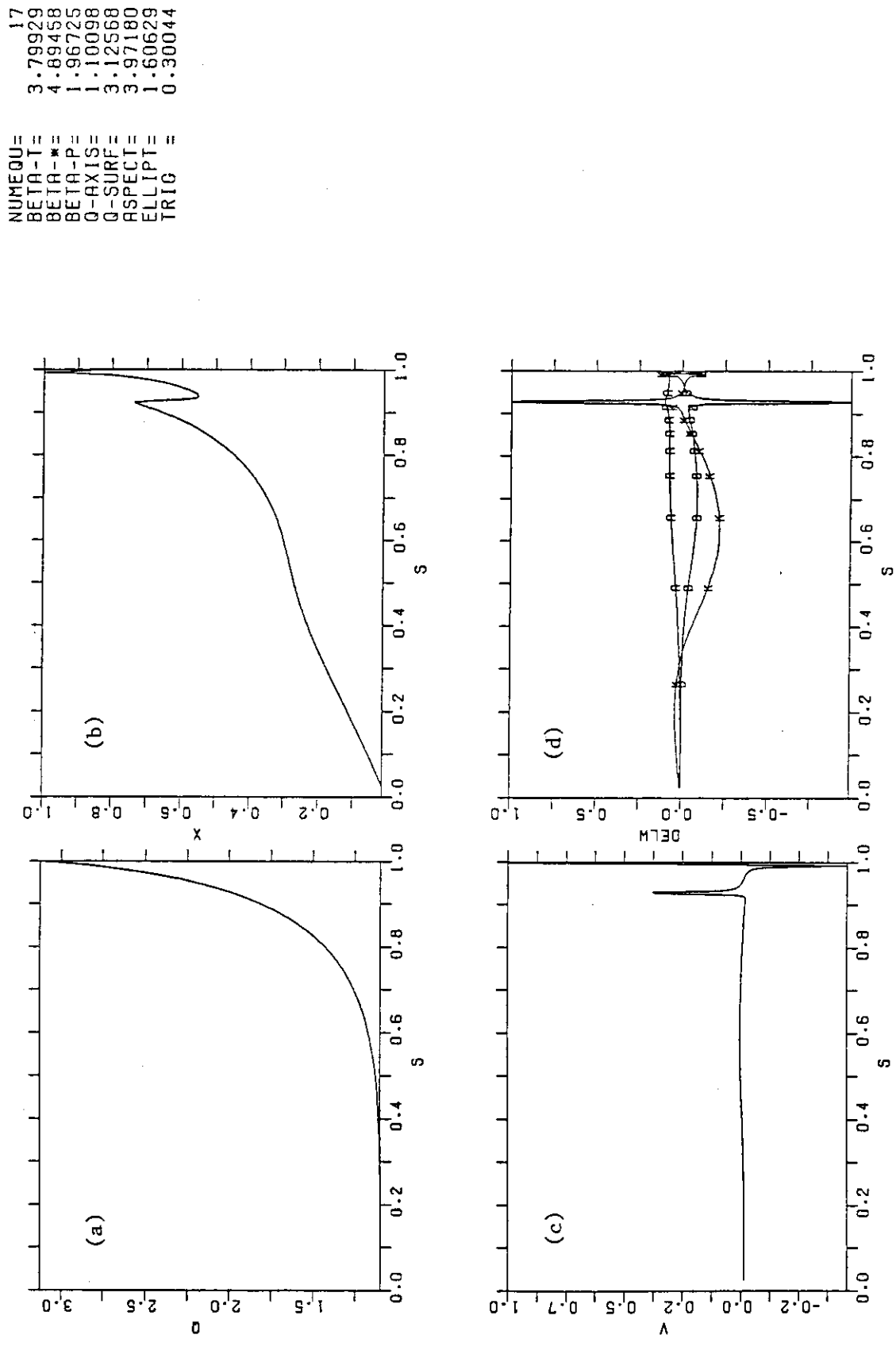

Fig.9 Mode structure near beta limit for the equilibrium Data 1.
β_t=3.80% and γ^2=1.45×10^{-5}.

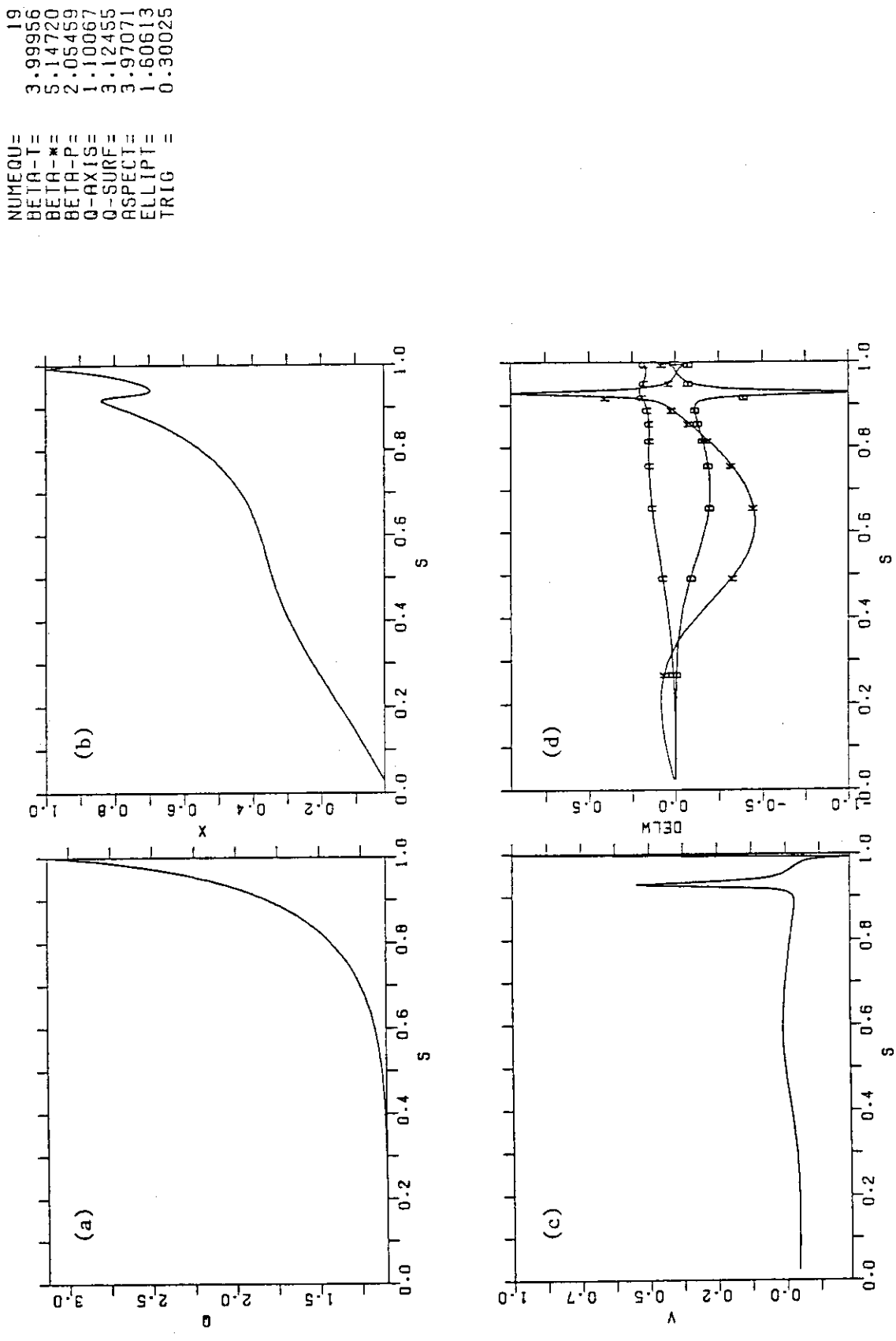

Fig.10 Mode structure of a weakly unstable n=1 kink mode for the equilibrium Data 1. β_t=4.00% and γ^2=1.16×10^{-4}.

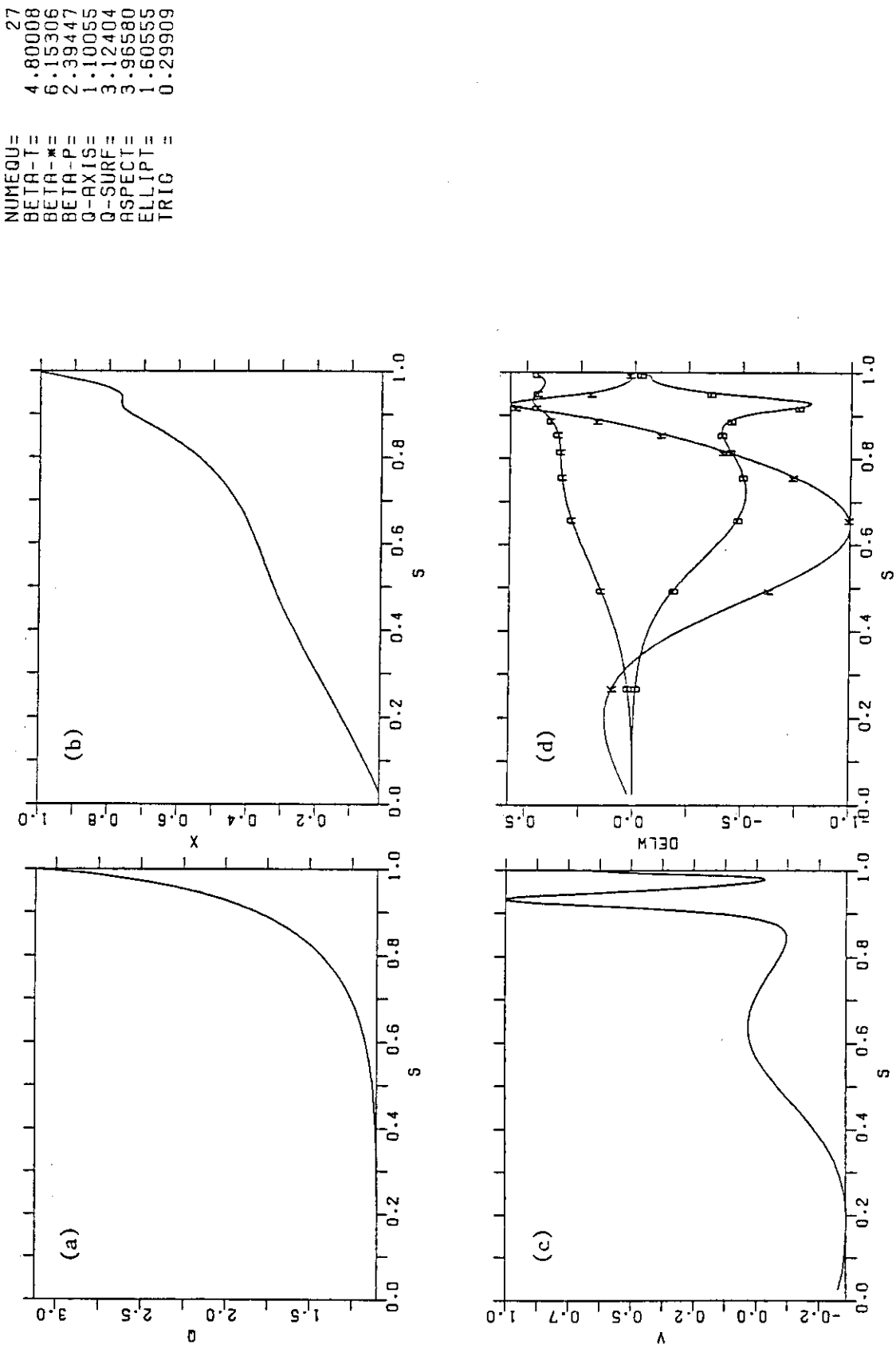

Fig.11 Mode structure of an unstable n=1 kink mode for the equilibrium Data 1. β_t=4.80% and γ^2=3.28×10^{-3}.

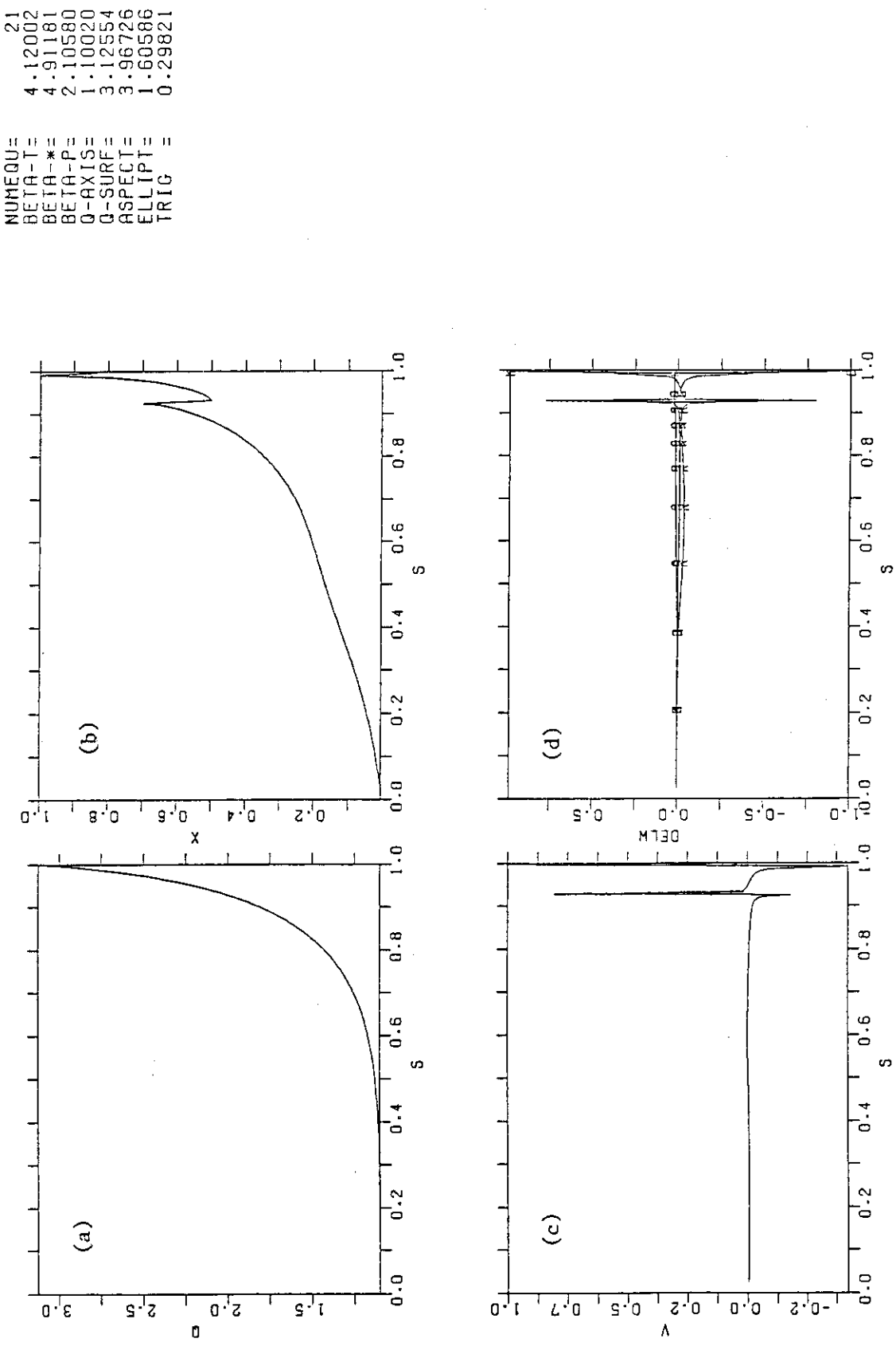

Fig.12 Mode structure of a stable n=1 kink mode for the equilibrium Data 2 β_t=4.12% and γ^2=8.91$\times$10^{-6}.

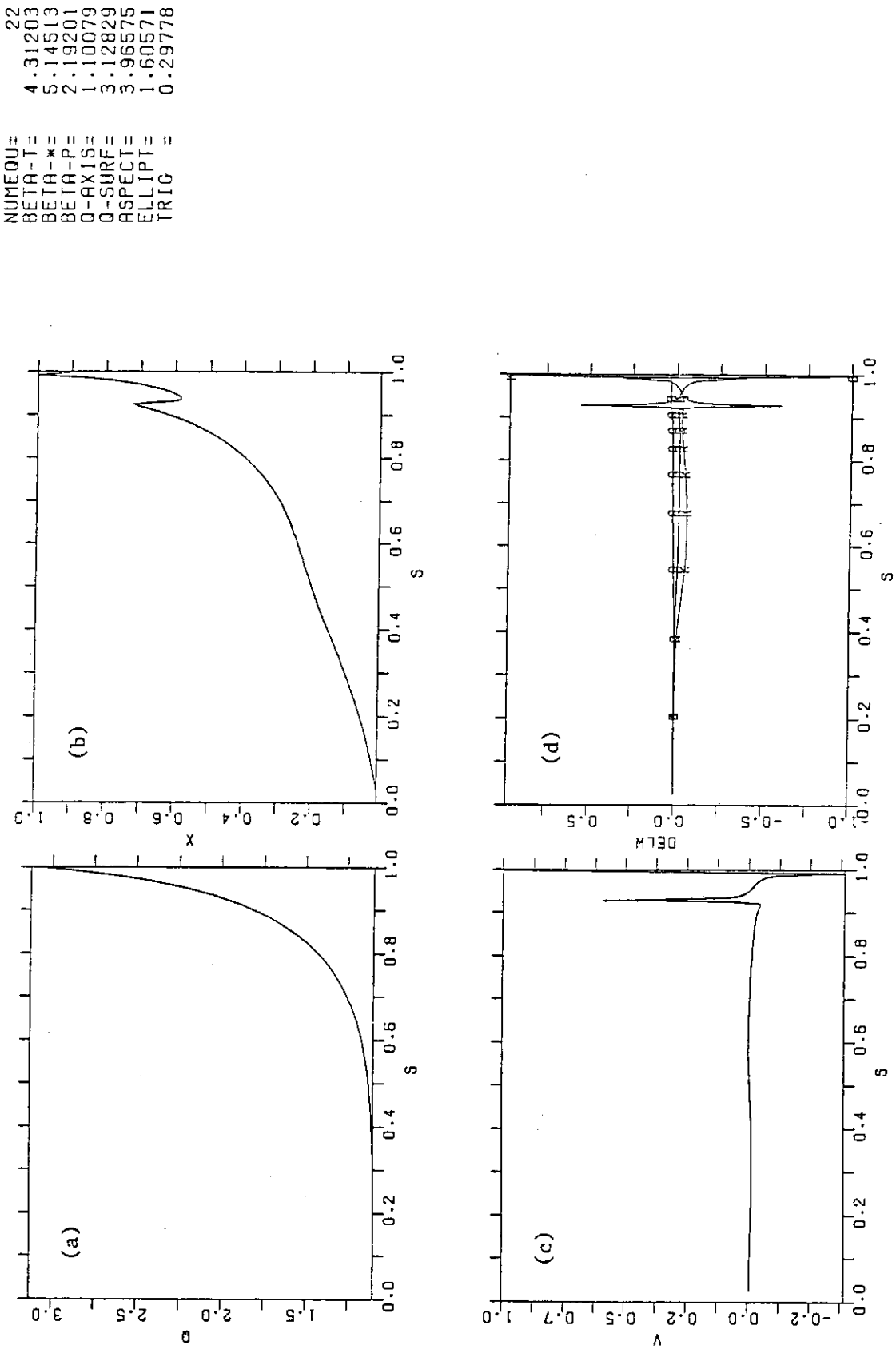

Fig.13 Mode structure of a weakly unstable n=1 kink mode (near beta limit) for the equilibrium Data 2. β_t=4.31% and γ^2=2.24×10^{-5}

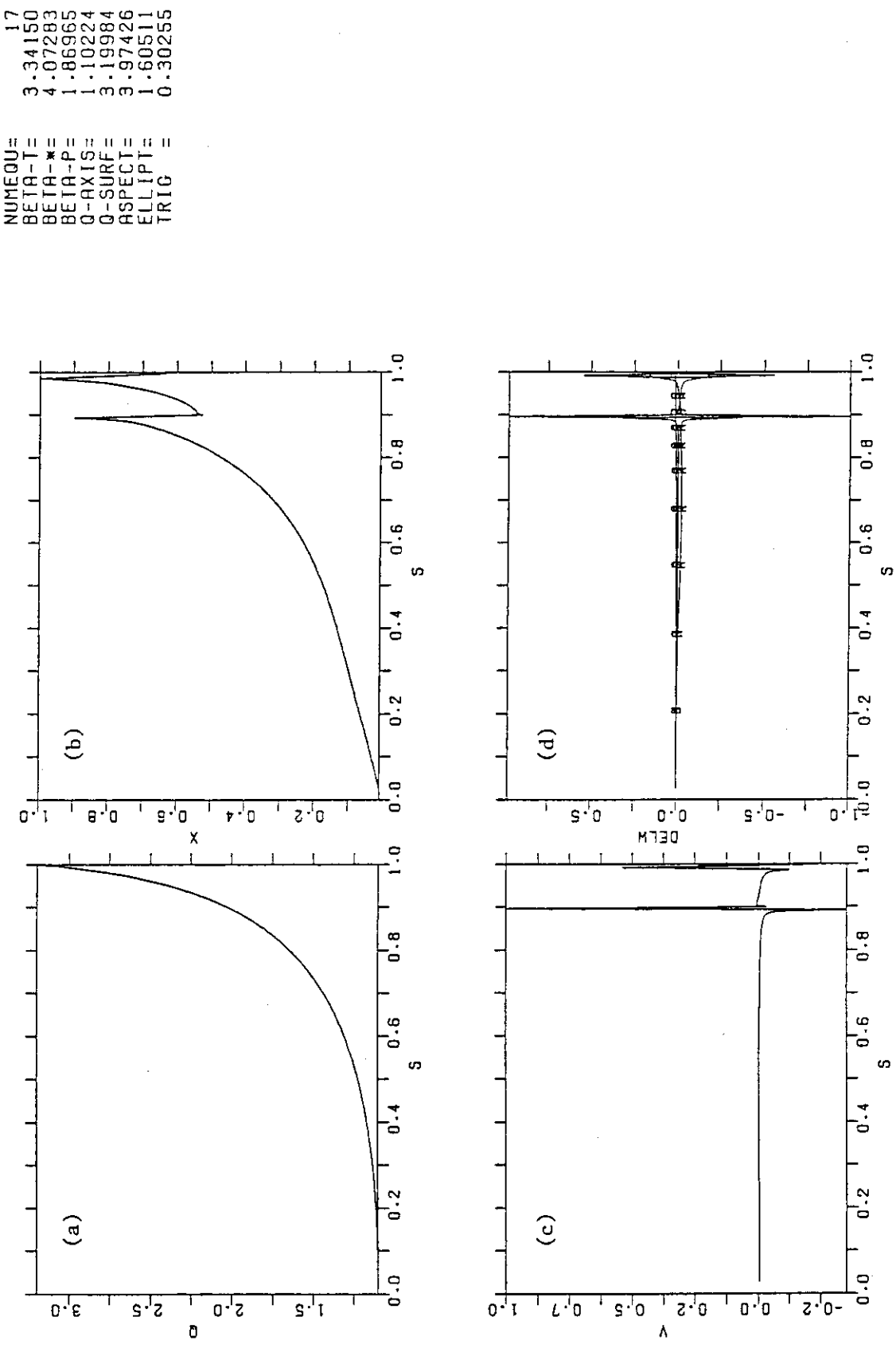

Fig.14 Mode structure of a stable n=1 kink mode for the equilibrium Data 3. β_t=3.34% and γ^2=4.06×10^{-6}.

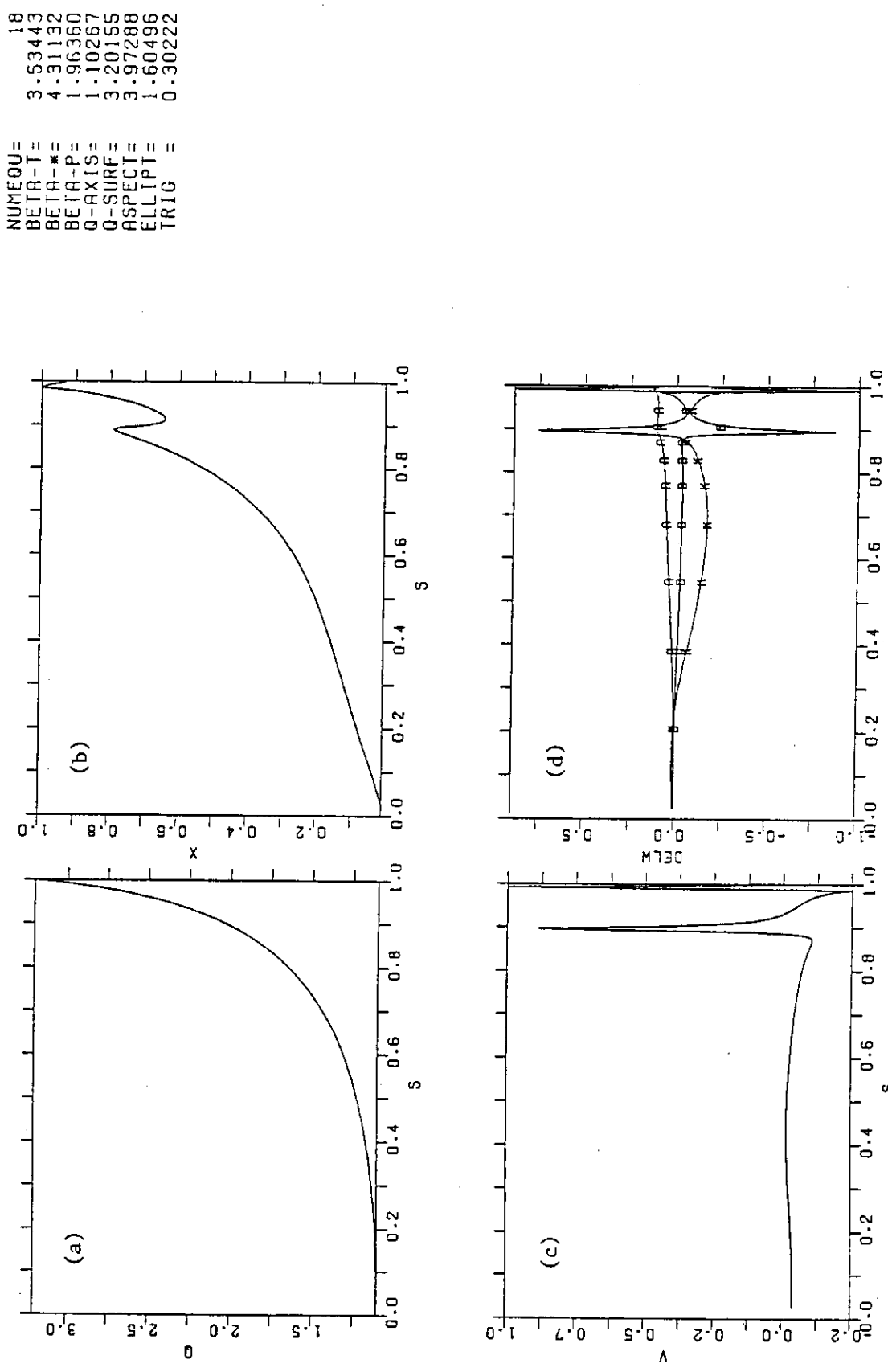

Fig.15 Mode structure of a weakly unstable n=1 kink mode for the equilibrium Data 3. β_t=3.53% and γ^2=4.24×10^{-5}.

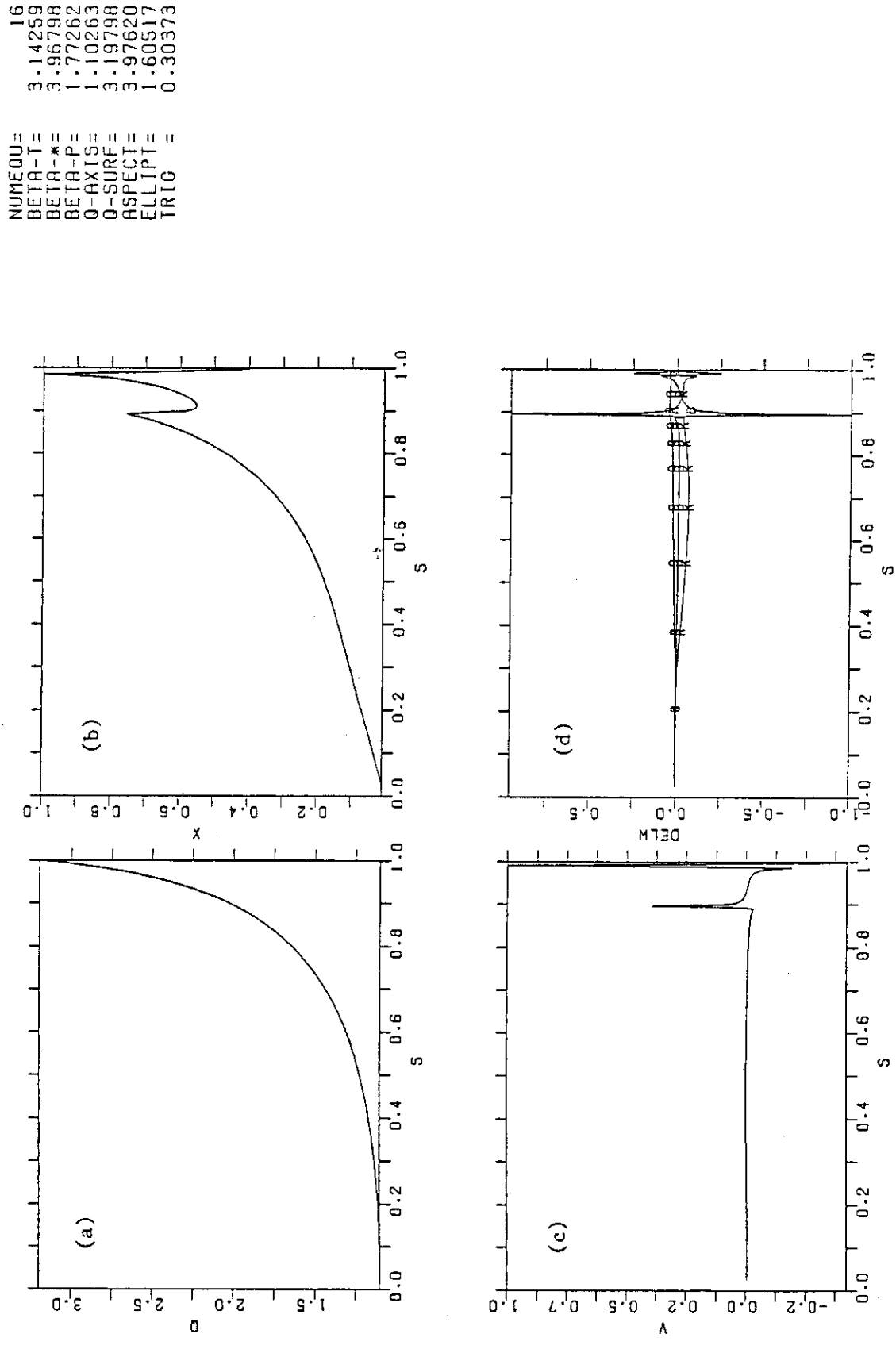

Fig.16 Mode structure near beta limit for the equilibrium Data 4.
β_t=3.14% and γ^2=9.45×10^{-6}.

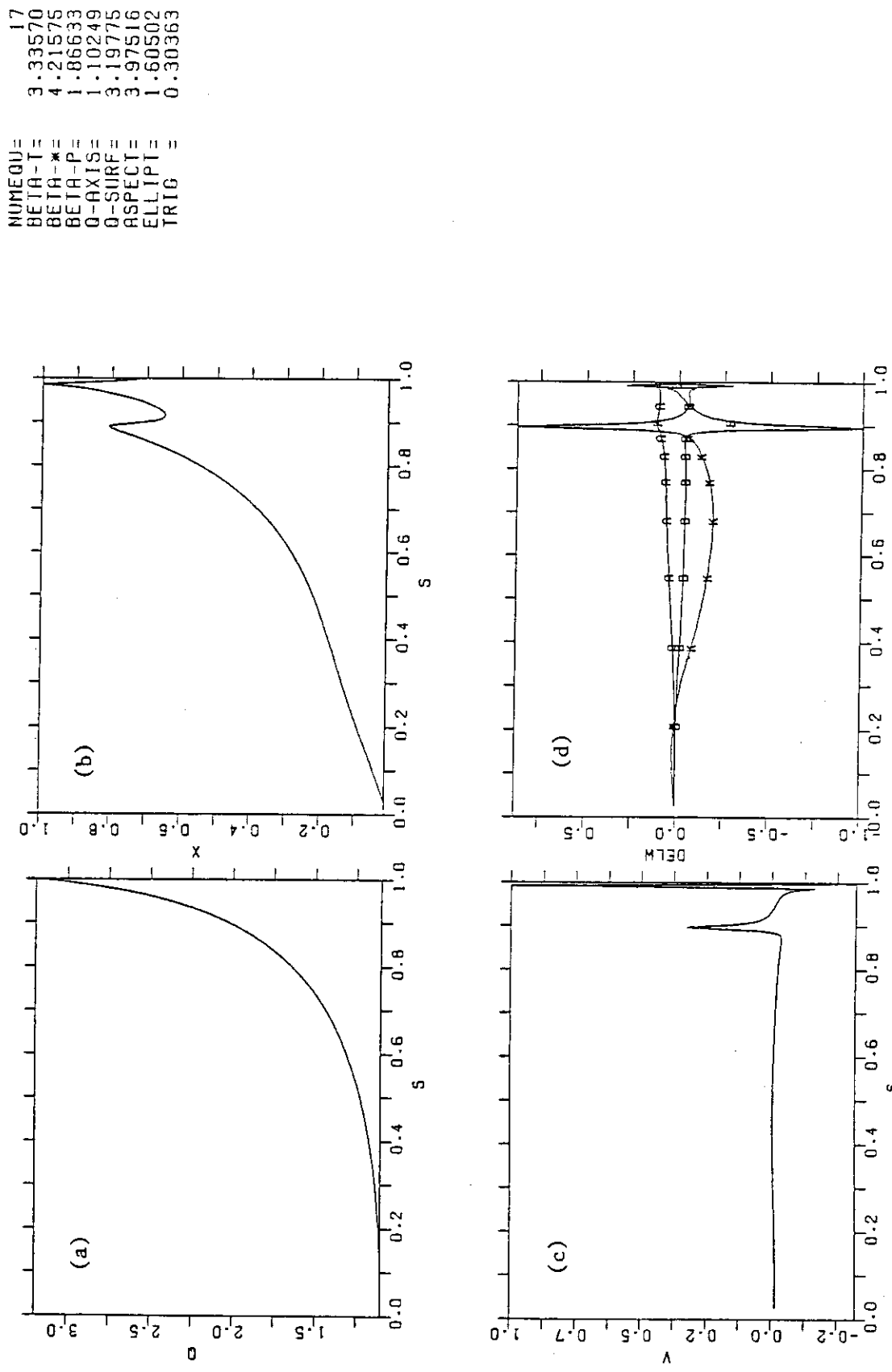

Fig.17 Mode structure of a weakly unstable n=1 kink mode for the equilibrium Data 4. β_t=3.34% and γ^2=4.53×10^{-5}.